nature portfolio

https://doi.org/10.1038/s41586-021-04321-5

Supplementary information

Selective sulfidation of metal compounds

In the format provided by the authors and unedited

Supplementary Information for **Selective Sulfidation of Metal Compounds**

Caspar Stinn[1] and Antoine Allanore[1]*

[1] Massachusetts Institute of Technology, Department of Materials Science and Engineering, Cambridge, MA, USA 02139-4307

*Corresponding author, allanore@mit.edu

Supplementary Materials

The following are included in the supplementary information below:

- Thermodynamic and solution framework for sulfidation
- Mass transfer considerations for measurement of sulfidation kinetics
- Determinization of critical gas flowrates for sulfidation
- Selective sulfidation capital cost analysis
- Selective sulfidation environmental impact analysis
- Discussion of supporting code and files for the technoeconomic analysis and life cycle assessment of selective sulfidation

The following are included in the separate supplementary data table:

- S1: Oxide reduction, sulfide reduction, and oxide sulfidation reactions in main Figure 1a
- S2: Parameters used to distinguish between kinetic and mass transport limitations to La_2O_3 sulfidation
- S3: Rare earth intragrain diffusivity comparison
- S4: Lanthanum oxide sulfidation conversion
- S5: Scandium oxide sulfidation intermediates
- S6: Zirconium oxide sulfidation products
- S7: Tungsten oxide sulfidation products
- S8: Strontium carbonate sulfidation products
- S9: Calcium carbonate sulfidation products
- S10: Physical separation of lithium ion battery elements facilitated by selective sulfidation
- S11: Lithium ion battery cathode selective sulfidation products
- S12: Lanthanum oxyfluoride synthesis and sulfidation products
- S13: Lanthanum phosphate sulfidation products
- S14: Capital cost curves and scaling factors
- S15: Monte Carlo parameters for sensitivity analysis of hydrometallurgy CAPEX
- S16: Chemistry-coupled Monte Carlo parameters for sensitivity analysis of sulfidation CAPEX, OPEX, and LCA
- S17: Chemistry-independent Monte Carlo parameters for sensitivity analysis of sulfidation CAPEX, OPEX, and LCA
- S18: Comparison of CAPEX, OPEX, and LCA burdens for sulfidation with and without pretreatments and CDSR
- S19: Operating conditions for zirconium-silicon separation from zircon via selective sulfidation
- S20: Operating conditions for iron-titanium separation from ilmenite via selective sulfidation

- S21: Operating conditions for rare earth elements separation from bastnaesite via selective sulfidation
- S22: Life cycle inventory for zirconium-silicon separation from zircon via selective sulfidation
- S23: Life cycle inventory for iron-titanium separation from ilmenite via selective sulfidation
- S24: Life cycle inventory for rare earth elements separation from bastnaesite via selective sulfidation
- S25: Allocation Data
- S26: Environmental impacts of sulfidation LCA case studies
- S27: Contributions to rare earth separation environmental impact with selective sulfidation
- S28: Thermodynamic data for technoeconomic and sustainability analysis of generalized process
- S29: Thermodynamic data for zirconium-silicon separation
- S30: Thermodynamic data for iron-titanium separation
- S31: Gas volume data
- S32: Equilibrium carbon-oxygen-sulfur gas phase interactions with CS_2 formation suppressed
- S33: Location factors for CAPEX

Thermodynamic and Solution Framework for Sulfidation

The thermodynamic framework for defining criteria for a sulfidation reaction to become thermodynamically spontaneous is outlined below. For any sulfidation reaction, there are two contributions to determining criteria for thermodynamic spontaneity: the pure compound sulfidation thermodynamics, and deviations from the pure compound sulfidation thermodynamics captured by solution thermodynamics. With this in mind, differences in sulfidation thermodynamics between a pure compound and that compound as it exists in natural minerals or recycling feedstocks are described entirely by deviations in the solution behavior. For sulfidation reactions where solution effect contributions to thermodynamic spontaneity are small, the sulfidation behavior may be viewed as reaction-dominated. Meanwhile, when the contributions to thermodynamic spontaneity from the sulfidation reaction are small compared to solution effects, the sulfidation reaction may be viewed as solution-dominated.

Sulfidation of a condensed metal-oxygen-sulfur reactant ($M_\beta O_\gamma S_\delta$) with elemental sulfur gas (S_2) to form a condensed product ($M_\epsilon O_\zeta S_\eta$) and gaseous sulfur dioxide (SO_2) is described by Eq. 1, where β, γ, δ, ϵ, ζ, and η are stoichiometric factors.

$$\frac{4\epsilon}{2\beta\eta+\gamma\epsilon-2\delta\epsilon-\beta\zeta} M_\beta O_\gamma S_\delta + S_2 = \frac{4\beta}{2\beta\eta+\gamma\epsilon-2\delta\epsilon-\beta\zeta} M_\epsilon O_\zeta S_\eta + \frac{2(\gamma\epsilon-\beta\zeta)}{2\beta\eta+\gamma\epsilon-2\delta\epsilon-\beta\zeta} SO_2 \quad (1)$$

At thermodynamic equilibrium, the relation between the standard Gibbs energy of reaction ($\Delta_r G°$), activity of the sulfidation reactant and product ($a_{M_\beta O_\gamma S_\delta}$ and $a_{M_\epsilon O_\zeta S_\eta}$ respectively), and gas partial pressures (P_{S_2}, P_{SO_2}) is described by Eq. 2, where R is the gas constant and T is the absolute temperature.

$$e^{\frac{-\Delta_r G°}{RT}} = \frac{P_{SO_2}^{\frac{2(\gamma\epsilon-\beta\zeta)}{2\beta\eta+\gamma\epsilon-2\delta\epsilon-\beta\zeta}} a_{M_\epsilon O_\zeta S_\eta}^{\frac{4\beta}{2\beta\eta+\gamma\epsilon-2\delta\epsilon-\beta\zeta}}}{P_{S_2} a_{M_\beta O_\gamma S_\delta}^{\frac{4\epsilon}{2\beta\eta+\gamma\epsilon-2\delta\epsilon-\beta\zeta}}} \quad (2)$$

Gas partial pressures may be isolated from condensed phase activities as follows:

$$\log_{10}\left(e^{\frac{\Delta_r G°}{RT}}\right) + \log_{10}\left(\frac{a_{M_\epsilon O_\zeta S_\eta}^{\frac{4\beta}{2\beta\eta+\gamma\epsilon-2\delta\epsilon-\beta\zeta}}}{a_{M_\beta O_\gamma S_\delta}^{\frac{4\epsilon}{2\beta\eta+\gamma\epsilon-2\delta\epsilon-\beta\zeta}}}\right) = \log_{10}\left(\frac{P_{S_2}}{P_{SO_2}^{\frac{2(\gamma\epsilon-\beta\zeta)}{2\beta\eta+\gamma\epsilon-2\delta\epsilon-\beta\zeta}}}\right) \quad (3)$$

$$\log_{10}\left(\frac{P_{S_2}}{P_{SO_2}^{\frac{2(\gamma\epsilon-\beta\zeta)}{2\beta\eta+\gamma\epsilon-2\delta\epsilon-\beta\zeta}}}\right) \equiv \psi \tag{4}$$

ψ is an equivalent P_{S_2}/P_{SO_2} ratio that accounts for the thermodynamic driving forces of product and reactant gases for reactions of different stoichiometries and valencies within $M_\beta O_\gamma S_\delta$ and $M_\epsilon O_\zeta S_\eta$, which in turn dictates the equilibrium extent of reaction following Le Chatelier's principle. ψ is the sum of reaction (ψ_{rxn}) and solution (ψ_{sol}) effects:

$$\psi = \psi_{rxn} + \psi_{sol} \tag{5}$$

$$\log_{10}\left(e^{\frac{\Delta_r G^\circ}{RT}}\right) = \psi_{rxn} \tag{6}$$

$$\log_{10}\left(\frac{a_{M_\epsilon O_\zeta S_\eta}^{\frac{4\beta}{2\beta\eta+\gamma\epsilon-2\delta\epsilon-\beta\zeta}}}{a_{M_\beta O_\gamma S_\delta}^{\frac{4\epsilon}{2\beta\eta+\gamma\epsilon-2\delta\epsilon-\beta\zeta}}}\right) = \psi_{sol} \tag{7}$$

ψ_{rxn} is tabulated from the standard Gibbs energy of reaction at a given temperature and pressure, thereby independent of whether the sulfidized species exists as a pure compound or within the compound matrix of a mineral or other feed. ψ_{rxn} is tabulated in Figure E2a for the sulfidation of some pure oxides, sulfates, and oxysulfides experimentally explored herein. Meanwhile, ψ_{sol} (Figure E2b) captures the contribution to sulfidation thermodynamics arising from differences in behavior of a compound in different feeds, as reflected by sulfidation reactant and product activities.

When $\psi_{rxn} \gg \psi_{sol}$, the sulfidation thermodynamics are reaction dominated, solution effects are minimal, and the sulfidation thermodynamics are well-described by those of the pure compound. Meanwhile, when $\psi_{rxn} \ll \psi_{sol}$, the sulfidation thermodynamics are solution dominated and reaction effects are minimal, the sulfidation thermodynamics are not well described by those of the pure compound, and knowledge of the solution behavior is essential to determine sulfidation spontaneity and sulfidation selectivity.

ψ serves as an effective P_{S_2} / P_{SO_2} ratio; yet for sulfidation reactions at different stoichiometries from one another, ψ is an inconsistent comparison, and sulfidation must be defined in the context of the actual P_{S_2} / P_{SO_2} ratio within the gas phase of the sulfidation reactor. The critical P_{S_2} / P_{SO_2} ratio for a sulfidation reaction to proceed to a given conversion is defined as $\left[\frac{P_{S_2}}{P_{SO_2}}\right]_{crit}$, and is determined from the gas phase thermodynamics of the system. At a given temperature and pressure, for a single gas phase consisting exclusively of sulfur and oxygen-containing species, where $M_\beta O_\gamma S_\delta$ and $M_\epsilon O_\zeta S_\eta$ are assumed to be non-volatile, one free intensive variable exists as stated via the Gibbs phase rule (Eq. 8), where F is a function of the number of chemical components (C) and number of phases present (P).

$$F = C - P + 2 \tag{8}$$

Therefore, P_{SO_2} exists as a function of P_{S_2}, as are ratios of P_{S_2} and P_{SO_2} such as ψ, ψ_{rxn}, ψ_{sol}, and $\left[\frac{P_{S_2}}{P_{SO_2}}\right]_{crit}$. Minimization of the system Gibb's energy may then be used to determine the equilibrium P_{SO_2} as a function of P_{S_2}, shown at 1 atmosphere of pressure at temperatures between 800°C and 1600°C in Figures E2c-E2d. The equilibrium P_{SO_2} / P_{S_2} ratio that satisfies ψ in Eq. 4 corresponds to $\left[\frac{P_{S_2}}{P_{SO_2}}\right]_{crit}$.

When $M_\beta O_\gamma S_\delta$ and $M_\epsilon O_\zeta S_\eta$ are assumed to be non-volatile and insoluble each with unit activity, a Kellogg diagram formalism may be used to graphically represent $\left[\frac{P_{S_2}}{P_{SO_2}}\right]_{crit}$ as the intersection of ψ, often referred to as phase domain boundaries, with the function of allowable gas

partial pressures, often referred to as the isobar line. Comparison of $\left[\frac{P_{S_2}}{P_{SO_2}}\right]_{crit}$ between different elements facilitates the construction of sulfidation series that describe the relative separation window for selective sulfidation of different components of a feed.

When carbothermically-driven sulfur reflux (CDSR) of SO_2 is employed, the gas phase will also include carbon-containing compounds. Similarly, if $M_\beta O_\gamma S_\delta$ and/or $M_\epsilon O_\zeta S_\eta$ are volatile, the gas phase will contain additional elements. P_{SO_2} ψ, ψ_{rxn}, and ψ_{sol} may still in principle be described as functions of P_{S_2}, so long as the Gibb's phase rule (Eq. 8) is followed.

Determinization of critical gas flowrates for sulfidation

The role of solid carbon on the carbothermically-driven sulfur reflux (CDSR) of SO_2 back into S_2 was modelled to determine the P_{S2}/P_{SO2} ratio in the active volume of the reactor. Steady state reactor conditions, a well-mixed gas phase, and a fixed reactor bed were assumed. Carbon-disulfide (CS_2) formation from the reaction of sulfur with elemental carbon was taken to be kinetically-suppressed[62], with other C-S-O reactions taken to be fast compared to the sulfidation reaction, existing at quasi-equilibrium. For different carbon sources or reactors with different transport phenomena, CS_2 formation may be present, yet may still be accounted for by following the framework below. Mass transfer limitations, including the effects of sintering, can be captured by scaling the sulfidation reaction rate constant by a kinetic effectiveness factor, derived following the methodology of the Theile modulus in heterogeneous catalysis[63]. By conducting a mass balance over the rate of gas introduction into the reactor, the rate of the sulfidation reaction, the rate of CDSR, and the rate of gas phase reactions with SO_2, the maximum average gas residence time to support sulfidation, known as the space time (τ_{space}^{max}), and its inverse known as the minimum space velocity (v_{space}^{min}), may be calculated as a function of sulfidation kinetics, reaction temperature, carbon feed content, and $[P_{S2}/P_{SO2}]_{crit}$.

The role of solid carbon on the carbothermically-driven sulfur reflux of SO_2 back into S_2 (Eq. 9) was modelled to determine the P_{S2}/P_{SO2} ratio in the active volume of the reactor ($[P_{S2}/P_{SO2}]_{reactor}$).

$$SO_2 + 2C = 2CO + \frac{1}{2}S_2 \tag{9}$$

Steady state reactor conditions, a well-mixed gas phase, and a fixed reactor bed were assumed. Carbon-disulfide (CS_2) formation was taken to be kinetically-suppressed[62], with other C-S-O reactions taken to be fast compared to the sulfidation reaction, existing at quasi-equilibrium. For different carbon sources or reactors with different transport phenomena, CS_2 formation may be present, yet may still be accounted for by following the framework below. For sulfidation of a trivalent metal oxide (M_2O_3) (Eq. 10) the amount of SO_2 entering the active volume of the reactor (N_{SO_2}) is a function of the rate of introduction of SO_2 from the gas inlet itself (U_{SO_2}), the rate of SO_2 generation from sulfidation of the trivalent metal oxide behind the reaction front (r_{SO_2}), and the reactor volume:

$$M_2O_3 + \frac{9}{4}S_2 = M_2S_3 + \frac{3}{2}SO_2 \tag{10}$$

$$N_{SO_2} = r_{SO_2}V + U_{SO_2} = \frac{2}{3}k\left(\frac{P_{S_2}}{RT}\right)^n V + U_{SO_2}[=]\frac{mol}{s} \tag{11}$$

Mass transfer limitations, including the effects of sintering, can be captured by scaling the rate constant (k) by a kinetic effectiveness factor, derived from $\hat{\sigma}$ as done from the Theile modulus of heterogeneous catalysis[63]. Meanwhile, the amount of S_2 entering the active volume of the reactor (N_{S_2}) is a function of the rate of introduction of S_2 from the gas inlet itself (U_{S_2}), the rate of S_2 consumption during sulfidation (r_{S_2}), and the reactor volume:

$$N_{S_2} = U_{S_2} - r_{S_2}V = U_{S_2} - k\left(\frac{P_{S_2}}{RT}\right)^n V[=]\frac{mol}{s} \tag{12}$$

In the absence of any carbothermic refluxing of SO_2 to S_2 or any gas phase reactions between S_2 and SO_2, assuming an ideal gas mixture the P_{S2}/P_{SO2} ratio entering the active volume of the reactor ($[P_{S2}/P_{SO2}]_{inlet}$) is calculated as follows:

$$\left[\frac{P_{S_2}}{P_{SO_2}}\right]_{inlet} = \frac{N_{S_2}}{N_{SO_2}} = \frac{U_{S_2} - k\left(\frac{P_{S_2}}{RT}\right)^n V}{\frac{2}{3}k\left(\frac{P_{S_2}}{RT}\right)^n V + U_{SO_2}} \tag{13}$$

The P_{S2}/P_{SO2} ratio in the active volume of the reactor ($[P_{S2}/P_{SO2}]_{reactor}$) is a function of $[P_{S2}/P_{SO2}]_{inlet}$, the carbon content described as a molar carbon to oxide feed ratio (N_C/N_{M2O3}), and the corresponding, temperature-dependent interactions between carbon and S-O gasses, dictated by thermodynamics (Table S32) if the gas phase is at a quasi-equilibrium compared to the rate of sulfidation and gas inlet:

$$\left[\frac{P_{S_2}}{P_{SO_2}}\right]_{reactor} = f\left(\left[\frac{P_{S_2}}{P_{SO_2}}\right]_{inlet}, \frac{N_C}{N_{M_2O_3}}\right) \tag{14}$$

For sulfidation to occur, $[P_{S2}/P_{SO2}]_{reactor}$ must exceed $[P_{S2}/P_{SO2}]_{crit}$. Employing Eqs. 13 and 14 and assuming an ideal gas phase, the minimum total gas volumetric flowrate (V_{min}) was found for sulfidation to occur as a function of temperature, $[P_{S2}/P_{SO2}]_{crit}$, N_C/N_{M2O3}, inlet gas partial (P_X) and total (P) pressures, and sulfidation rate constant k:

$$\dot{V}_{min} = f\left(T, \left[\frac{P_{S_2}}{P_{SO_2}}\right]_{inlet}, \frac{N_C}{N_{M_2O_3}}, P_X, P, k\right)[=]\frac{m^3}{s} \tag{15}$$

The maximum average gas residence time, known as the space time (τ_{space}^{max}), and its inverse known as the minimum space velocity (v_{space}^{min}) are determined from $\dot{V}_{min}$ and the reactor volume, V, as follows:

$$\tau_{space}^{max} = \frac{1}{v_{space}^{min}} = \frac{V}{\dot{V}_{min}}[=]s \tag{16}$$

Mass Transfer Considerations for Measurement of Sulfidation Kinetics

Equations 17-19 are taken to describe the net sulfidation of lanthanum oxide and gaseous diatomic sulfur with inclusion of a carbon source. While other gas reactions were also present, the species involved were found to be dilute and their role in the sulfidation kinetics was therefore ignored.

$$La_2O_3 + \frac{25}{12}S_2 = \frac{2}{3}La_3S_4 + \frac{3}{2}SO_2 \tag{17}$$

$$\frac{2}{3}La_3S_4 + \frac{1}{6}S_2 = La_2S_3 \tag{18}$$

$$SO_2 + 2C = 2CO + \frac{1}{2}S_2 \tag{19}$$

La_3S_4 is a "lower" sulfide product that occurs prior to the formation of La_2S_3, in addition to the formation of an intermediate oxysulfide, La_2O_2S. With this proposed mechanism, the reaction of La_3S_4 to La_2S_3 is indiscernible in IR product gas analysis (see Methods) due to the fact that no additional oxygen-containing gasses would be liberated during the sulfidation of La_3S_4 to La_2S_3, while the reactions of La_2O_3 to La_2O_2S and La_2O_2S to La_3S_4 are indistinguishable in the gas signal due to their simultaneous occurrence within the packed bed reactor. Carbothermic refluxing of SO_2 to S_2 (Eq. 19) is taken to be fast compared to sulfidation. The sulfidation reaction is taken to be zero order with regard to concentration of the solid, and the gasses are assumed to form an ideal gas mixture, resulting in a rate law of the following form on a per unit volume basis, where $r_{La_3S_4}$ is the rate of formation of La_3S_4, r_{SO_2} is the rate of formation of SO_2, r_{CO} is the rate of formation of CO, r_O is the corresponding rate of oxygen liberation during sulfidation, k is the observed reaction rate constant, n is the reaction order in S_2, P_{S_2} is the S_2 partial pressure, R is the gas constant, and T is the absolute temperature:

$$r_{La_3S_4} = \frac{4}{9} r_{SO_2} + \frac{8}{9} r_{CO} = \frac{18}{25} k \left(\frac{P_{S_2}}{RT}\right)^n [=] \left(\frac{mol_{La_3S_4}}{m^3}\right) s^{-1} \quad (20)$$

$$r_O = \frac{9}{2} r_{La_3S_4} = \frac{81}{25} k \left(\frac{P_{S_2}}{RT}\right)^n [=] \left(\frac{mol_O}{m^3}\right) s^{-1} \quad (21)$$

$$k[=] \left(\frac{m^3}{mol}\right)^{n-1} s^{-1} \quad (22)$$

Considering the density of the rare earth oxide, the reaction rate (r') can also be described on an oxide mass basis with the following form, where ρ_B is the bulk density of the solid pellet, $\rho_{La_2O_3}$ is the density of the oxide, and ϵ is the porosity of the pellet:

$$r'_{La_3S_4} = \frac{4}{9} r'_{SO_2} + \frac{8}{9} r'_{CO} = \frac{18}{25} \frac{k}{\rho_B} \left(\frac{P_{S_2}}{RT}\right)^n [=] \left(\frac{mol_{La_3S_4}}{kg_{La_2O_3}}\right) s^{-1} \quad (23)$$

$$r'_O = \frac{9}{2} r'_{La_3S_4} = \frac{81}{25} \frac{k}{\rho_B} \left(\frac{P_{S_2}}{RT}\right)^n [=] \left(\frac{mol_O}{kg_{La_2O_3}}\right) s^{-1} \quad (24)$$

$$k' = \frac{k}{\rho_B} [=] \left(\frac{m^3}{mol}\right)^{n-1} \frac{m^3}{kg} s^{-1} \quad (25)$$

$$\rho_B = \rho_{La_2O_3}(1 - \epsilon) \quad (26)$$

Considering surface area of the rare earth oxide, the reaction can be described on an oxide surface area basis with the following form, where S is the specific surface area:

$$r''_{La_3S_4} = \frac{4}{9} r''_{SO_2} + \frac{8}{9} r''_{CO} = \frac{18}{25} \frac{k}{\rho_B S} \left(\frac{P_{S_2}}{RT}\right)^n [=] \left(\frac{mol_{La_3S_4}}{m^2_{La_2O_3}}\right) s^{-1} \quad (27)$$

$$r''_O = \frac{9}{2} r''_{La_3S_4} = \frac{81}{25} \frac{k}{\rho_B S} \left(\frac{P_{S_2}}{RT}\right)^n [=] \left(\frac{mol_O}{m^2_{La_2O_3}}\right) s^{-1} \quad (28)$$

$$k'' = \frac{k}{S_{Ln_2O_3}\rho_B} [=] \left(\frac{m^3}{mol}\right)^{n-1} \frac{m}{s} \quad (29)$$

In general, the initial rate of reaction and partial pressures are typically utilized to determine reaction kinetics. The observed reaction order and rate constant can be found by fitting IR gas signal data for sulfur and oxygen containing species to the following relation, where $m_{La_2O_3}$ is the initial mass of oxide:

$$\ln r'_O = n \ln \left(\frac{P_{S_2}}{RT}\right) + \ln \left(\frac{81}{25} \frac{k m_{La_2O_3}}{\rho_{Ln_2O_3}(1-\epsilon)}\right) \quad (30)$$

The observed activation energy (E_A) and Arrhenius pre-exponential factor (A_r) are found by fitting k versus T^{-1} to the natural log of the Arrhenius equation:

$$\ln k = \frac{-E_A}{RT} + \ln A_r \quad (31)$$

However, for a fluid-solid reaction, the observed initial rate of reaction does not inherently reflect the intrinsic chemical rate due to the presence of internal (within the porous solid) and external (to the surface of the porous solid) mass transfer limitations[25,63,64]. In order the measure intrinsic chemical kinetics, experiments must be performed in regimes where both internal and external mass transfer limitations are shown to be negligible.

Ishida and Wen[67] proposed that the impact of external mass transfer effects on a fluid-solid reaction is described by the pellet Sherwood number (Sh), where k_c is the convective mass transfer coefficient, d_p is the effective diameter of the pellet, and D_{AB} is the molecular diffusivity:

$$Sh = \frac{k_c d_p}{D_{AB}} \quad (32)$$

Sohn and Szekely revisited this Sherwood criteria for fluid-solid reactions, showing that for a modified Sherwood number (Sh') greater than 30, external mass transfer has no effect on the observed rate of reaction, where D_E is the effective diffusivity[68]:

$$Sh' = Sh\frac{D_{AB}}{D_E} \tag{33}$$

The effective diffusivity includes both Knudsen and molecular contributions, and is described using the Bosanquet interpolation formula[65], where D_{Ek} is the effective Knudsen diffusivity and D_{Em} is the effective molecular diffusivity:

$$D_E = \frac{1}{\frac{1}{D_{Ek}}+\frac{1}{D_{Em}}} \tag{34}$$

The effective Knudsen and molecular diffusivities within a pellet are calculated as follows[65], where r_g is the radius of a grain within the pellet, τ is the tortuosity of within the pellet, and m_A is the molar mass of the diffusing species:

$$D_{Ek} = \frac{r_g\epsilon}{\tau(1-\epsilon)(1+\frac{\pi}{8})\sqrt{(\frac{8m_A}{\pi RT})}} \tag{35}$$

$$D_{Em} = \frac{\epsilon D_{AB}}{\tau} \tag{36}$$

The molecular diffusion coefficient of a species in a carrier gas can be estimated using the Chapman-Enskog theory,[71] where c_1 is a constant, m_B is the molar mass of the carrier gas, P is the pressure, σ_{AB} is the collision diameter, Ω is a dimensionless energy parameter:

$$D_{AB} = \frac{c_1 T(\frac{1}{m_A}+\frac{1}{m_B})}{P{\sigma_{AB}}^2\Omega} \tag{37}$$

In practice, the Sherwood number, defined as the ratio of convective to diffusive mass transport, is problematic to calculate directly due to difficulty in determining the convective mass transfer coefficient. However, the Sherwood number can be related to the Reynolds number (Re) and Schmidt number (Sc) using relations such as the Frössling correlation[63]:

$$Sh = 2 + 0.6Re^{\frac{1}{2}}Sc^{\frac{1}{3}} \tag{38}$$

The Reynolds number[72], defined as the ratio of inertial and viscous forces in the fluid, is calculated from the fluid velocity (U), the effective spherical particle diameter[63] (L), and the fluid kinematic viscosity (ν):

$$Re = \frac{UL}{\nu} \tag{39}$$

In general, relations for Sherwood number and Reynolds number are dependent on the reactor geometry. The kinematic viscosity of a gas is described by the following[69], where c_2 is a constant, x_A and x_B are the mole fractions of species A and B respectively, and ρ_g is the density of the gas:

$$\nu = c_2\frac{\sqrt{(x_A m_A + x_B m_B)T}}{\rho_g {\sigma_{AB}}^2} \tag{40}$$

The Schmidt number, defined as the ratio of momentum to mass diffusivity, is calculated as follows[63]:

$$Sc = \frac{\nu}{D_{AB}} \tag{41}$$

To characterize the effect of internal mass transfer limitations on fluid-solid reactions, Sohn and Szekely proposed a generalized fluid-solid reaction modulus relating chemical reaction rates to pore diffusion rates[65], serving in a similar role to the Theile modulus of heterogeneous catalysis. The generalized fluid-solid reaction modulus ($\hat{\sigma}$) is defined as follows, where V_p and V_g are the volumes of the pellet and a grain within the pellet respectively, A_p and A_g are the surface areas of the pellet and a grain within the pellet respectively, C_A is the concentration of the

reacting species in the fluid, F_p and F_g are geometric factors for the pellet and a grain within the pellet respectively, and D_E is the effective diffusivity:

$$\hat{\sigma} = \frac{V_p}{A_p}\sqrt{\frac{(1-\epsilon)k''\left(\frac{P_{S_2}}{RT}\right)^{n-1}F_pA_g}{2D_EF_gV_g}} \tag{42}$$

For conditions where $\hat{\sigma}^2 < 0.01$ and $Sh' > 30$, the surface reaction is kinetically-limited and the observed surface reaction rate over the entire conversion range is equal to the initial rate and reflects the intrinsic chemical kinetics[25,65] when intragrain diffusion limitations are ignored.

To determine if intragrain diffusion limitations are minimal, a modified mass transfer Biot number $\hat{\sigma}_g$ is proposed by Sohn and Szekely[66], where D_g is the reacting gas-phase species diffusivity in the solid:

$$\hat{\sigma}_g{}^2 = \frac{k''\left(\frac{P_{S_2}}{RT}\right)^{n-1}V_g}{2D_gA_g} \tag{43}$$

The mass transfer Biot number is classically defined as the ratio of the mass transfer resistance inside of a pellet to that on the surface of the pellet, here redefined for a single grain. For conditions where $\hat{\sigma}_g{}^2 < 1$, intragrain diffusion effects are negligible compared to the reaction rate at the reaction front[66]. In practice, D_g for sulfur is often unknown for many sulfides at high temperatures. Setting $\hat{\sigma}_g{}^2$ equal to one, a minimum D_g to avoid intragrain diffusion limitation can be found for a given particle reaction rate and particle geometry:

$$\left[D_g\right]_{min} = \frac{k''\left(\frac{P_{S_2}}{RT}\right)^{n-1}V_g}{A_g} \tag{44}$$

Following the principles of thermal activation of diffusion[73], D_g can be estimated from similar solid state systems, here rare earth oxides[70]. Literature parameters utilized in all mass transfer calculations are outlined in Tables S2-S3. Together, when $\hat{\sigma}^2 < 0.01$, $Sh' > 30$, and $\hat{\sigma}_g{}^2 < 1$ (alternatively $D_g > \left[D_g\right]_{min}$), external and internal mass transfer limitations are negligible throughout the oxide being sulfidized and the observed kinetics are the intrinsic chemical reaction kinetics[25]. These conditions are met in our experiments (see Figure E4 and Tables S2-S3). Therefore, our observed sulfidation kinetics are equal to the intrinsic chemical reaction rate.

Technoeconomic Assessment

Capital and Operating Costs

To understand the economic implications of material processing via selective sulfidation, the capital and operating costs (CAPEX and OPEX respectively) of four generic material separations are estimated. These are selective sulfidation with and without feed pretreatments, each with and without carbothermically-driven sulfur reflux (CDSR). Process flow diagrams are included in Figures E8 and S1-S3. For selective sulfidation and physical separation without pretreatment, the following process blocks are employed: nitrogen separation from air for sulfidation carrier gas production, sulfidation in a multihearth fluidized bed reactor, comminution, physical separation via froth flotation, and waste gas stream handling via a cyclone separator, followed by either electrostatic solids precipitator and dual alkali scrubbing (when the carbothermically-driven sulfur reflux, CDSR, is utilized in sulfidation) or sulfuric acid production (No CDSR). Materials containing impurities such as normally occurring radioactive elements or anions other than oxygen and sulfur may require additional pretreatments prior to selective sulfidation. The CAPEX and OPEX of selective sulfidation with some possible material feed preparation / pretreatment steps are also considered, such as feed drying, calcination for defluorination of fluorocarbonate minerals or lithium ion battery electrolytes and oxidation of mixed metal compounds such as rare earth magnets, sulfidation for dephosphorization of phosphate minerals and dethoriation of rare earth concentrates, and

sulfidation/calcination for sintering of material feeds too finely ground for effective liberation and physical separation of sulfide precipitants post selective sulfidation. Operating conditions for selective sulfidation are included in Tables S16-S17.

The CAPEX of equivalent generic hydrometallurgical processes are estimated as a point of comparison to selective sulfidation. Their flowsheets consist of acid roasting for impurity removal and formation of soluble metal compounds, gas treatment via acid plant, leaching of the target elements, solvent extraction for metal element separation, and precipitation of product metal compounds, with operating conditions reported in Table S15. Four scenarios are considered: pulsed-column and mixer-settler liquid-liquid contactors, each at separation factors of 1.5 and 10,000 corresponding to f and d-block element separations respectively. Generally, the liquid-liquid separation effectiveness for two metals (M_1 and M_2) achieved by an aqueous-organic separation system is described by the separation factor (β), where D is the distribution ratio, x is the concentration, and γ is the activity coefficient, where A and O denotes the aqueous and organic phases respectively[8]:

$$\beta_{M_1/M_2} = \frac{D_{M_1}}{D_{M_2}} = \frac{\frac{x_{M_1}^{(O)}\gamma_{M_1}^{(O)}}{x_{M_1}^{(A)}\gamma_{M_1}^{(A)}}}{\frac{x_{M_2}^{(O)}\gamma_{M_2}^{(O)}}{x_{M_2}^{(A)}\gamma_{M_2}^{(A)}}} \quad (45)$$

At dilute concentrations, γ is approximated as unity. Generally, industrially-realized separation factors range from near one for many binary rare earth separations into the thousands and tens of thousands for some binary transition metal separations[8,75,77].

The OPEX for a generic hydrometallurgical process is not estimated, as it is known to vary strongly with location, feed solubility, liquid-liquid extractor chemistry, and liquid-liquid contactor design[8]. The variation of the contributions to OPEX are not well-quantified in academic literature. Therefore, comparison of OPEX between processes based on sulfidation and liquid-liquid hydrometallurgy is presently not attempted.

For the generic hydrometallurgical and selective sulfidation based pathways, the feedstock is assumed to be an equimolar mixture of two metal oxides, with chemistry represented by copper(I) oxide (Cu_2O), nickel(II) oxide (NiO), or neodymium(III) oxide (Nd_2O_3), as discussed later in *Sensitivity Analysis*. Feed capacities ranging from 10,000 to 1,000,000 tonnes per year are considered. Product purities of 99% are assumed following separation of the binary oxide feed. The economics of upstream beneficiation and comminution processes and downstream metal reduction processes are taken to be largely unchanged for either the solvent extraction or selective sulfidation pathways.

For cost analysis, we utilize Class 4 (+/- 30% accuracy) estimates as described by the American Association of Cost Engineers (AACE) International[48,76,79]. Class 4 CAPEX estimates employ scaling relations based on individual unit operations, making them useful for high-level comparison of technologies. A typical scaling relation for CAPEX (C) is as follows, where *a* is a pre-exponential factor and P is the relevant metric by which the operation is scaled (typically size or throughput), and n is an exponent corresponding to the economy of scale[76]:

$$C = aP^n \quad (46)$$

Class 4 CAPEX estimates do not replace the insight gained from detailed design work however; they only illustrate general trends. Nevertheless, solvent extraction is a well-established technology that affords a good understanding of its capital framework and individual unit operations. Meanwhile, selective sulfidation as envisioned herein employs a high temperature fluidized bed multihearth reactor, such as currently employed for calcination, and orthodox physical separations, all relying on well-documented unit operations with quantifiable economics[48]. Therefore, a Class 4 CAPEX analysis for selective sulfidation and solvent extraction is based in a convention that supports reasonable comparison of hypothetical process economics.

Scaling relations for capital cost are determined using the factorial method[48,76], described below. The total fixed capital cost, or total module cost (C_T) of a processing block may be determined through the following relation:

$$C_T = (LF * TM * BM * PM * LM * FOB)\left(\frac{I}{I_R}\right)P^n \quad (47)$$

LF, TM, BM, PM, LM, and FOB are scaling preexponential factors. I is the cost index for the year utilized for the estimate, here the 2020 Chemical Engineering Plant Cost Index (CEPCI), whereas I_R is the reference cost index. FOB corresponds to the free on board scaling factor to determine the purchase price (C_{FOB}) of a given piece of equipment as a function of the relevant scaling metric and herein includes material factors:

$$C_{FOB} = (FOB)\left(\frac{I}{I_R}\right)P^n \quad (48)$$

LM corresponds to the scaling factor to account for instruments and buildings within the battery limit. PM corresponds to the scaling factor to include taxes, freight, and insurance associated with installation of the process block. The physical module cost (C_{PM}) of the process block is described as follows:

$$C_{PM} = (PM * LM * FOB)\left(\frac{I}{I_R}\right)P^n \quad (49)$$

The ISBL cost (C_{ISBL}) of the process is taken as the sum of C_{PM} for the processing blocks:

$$C_{ISBL} = \sum\left((PM * LM * FOB)\left(\frac{I}{I_R}\right)P^n\right) \quad (50)$$

TM and BM correspond to scaling factors for offsites/indirect/field expenses and design/engineering/contingency respectively. LF is a location factor to scale CAPEX between different geographic regions. The total fixed capital cost, or total module cost, (C_{FC}) of the full process may be described as the sum of the total module costs of each process block:

$$C_{FC} = \sum\left((LF * TM * BM * PM * LM * FOB)\left(\frac{I}{I_R}\right)P^n\right) \quad (51)$$

TM, BM, PM, LM, FOB, P, I, I_R and n for relevant processing operations[48] for both the hydrometallurgical and sulfidation processing pathways are included in Table S14. LF for different geographies[76] are included in Table S33.

Operating costs (OPEX) of the generic selective sulfidation processes described above and illustrated in Figure E8 and S1-S3 above are estimated from reagent, utility, and waste treatment prices, correlations for labor costs with relevant chemical process unit operations, correlations for management and overheads with labor cost, and correlations for maintenance costs with CAPEX, as described in Table S17. Revenue credits from byproduct sulfuric acid production are excluded in OPEX analysis of the generic process, but may be included in economic evaluation of a real project. OPEX as estimated herein does not include processing steps upstream of selective sulfidation and its supporting pretreatments, such as mining and preliminary comminution / mineral dressing in primary production from ores, or material collection and crushing / disassembly in secondary materials production from recycled materials. These upstream steps are not considered since they are necessary regardless of the downstream materials separation technique employed (leaching, solvent extraction, pyrometallurgical smelting, selective sulfidation, etc.), and may or may not be conducted at the same facility as downstream materials processing. Likewise, differences in costs between established and greenfield facilities are not considered herein.

For the generic binary separation of equimolar mixed metal oxides, the selective sulfidation pathway is predicted to exhibit a 65-90% reduction in CAPEX compared to hydrometallurgical separation at separation factors of 1.5-10,0000, representative of solvent extraction for f-block elements and d-block elements separation respectively[8] (Figure 3a). The OPEX of selective sulfidation is predicted to be on the order of

$50, $100, and $300 per tonne of feed at feed capacities of 1,000, 100, and 10 kilotonnes per year respectively. Attribution of CAPEX and OPEX to individual processing steps are presented in Figures S5-S6. Individual pretreatment steps for feed drying, sintering, and roasting/calcination each marginally increase the CAPEX and OPEX of selective sulfidation by 10% to 20% (Figure E9, Table S18). While preliminary CAPEX and OPEX estimates are promising, to understand the profitability of a given materials separation process utilizing selective sulfidation, detailed design considering geographic-specific factors (ore grade and impurities, labor costs and utilization, trends in automation, greenfield versus established facility, etc.) and further refinement of sulfidation operating conditions and chemistries will be necessary.

Sensitivity Analysis

Sensitivity analysis for OPEX and CAPEX is conducted via Monte Carlo simulation[76] at selective sulfidation feed capacities of 10,000, 100,000 and 1,000,000 tonnes of feed per year. At each feed capacity, 360,000 iterations of the CAPEX and OPEX models were conducted. Operating parameters and conditions, reagent costs, labor requirements and costs, yearly maintenance cost as a fraction of CAPEX, Class 4 CAPEX error (+/-30%), and geographic scaling factors were each randomly varied using continuous triangular distributions centered around known or calculated values, as outlined in Tables S15 and S17. When uninformed by literature, upper and lower bounds for triangular distributions[76] were taken as -50% to +100% of the base value. Thermodynamic inputs for mass and energy balances and chemistry-specific operating conditions were randomly varied using coupled discrete, uniform distributions across the sulfidation chemistries of copper(I) oxide (Cu_2O), nickel(II) oxide (NiO), or neodymium(III) oxide (Nd_2O_3), as outlined in Table S16.

From the Monte Carlo simulation, error in CAPEX and OPEX parameters are taken as +/- one standard deviation from the mean of the distribution. For CAPEX, the error was larger as a percentage of the mean for the generic hydrometallurgical routes than the generic sulfidation routes due to a stronger dependence on chemical factors, namely feed concentration. For selective sulfidation, feed concentration is ill-defined, since the solid feed is introduced directly to the sulfidation reactor. Meanwhile in the hydrometallurgical pathway, the solid feed is dissolved prior to pretreatment, and the concentration of the feed was varied during Monte Carlo simulation. The resultant larger uncertainty highlights the difficulty of describing the economic framework of a generic hydrometallurgical process. Nevertheless, the predicted reduction to CAPEX by adopting selective sulfidation and physical separation in place of hydrometallurgical chemical separation is resilient to these chemistry uncertainties.

Environmental Assessment

Goal and Scope

Selective sulfidation for f-block and d-block element separation embodies a shift from hydrometallurgy and chemical separations to pyrometallurgy and physical separations. To understand the environmental impacts of material processing via selective sulfidation, the environmental impacts of four generic material separations are analyzed using life cycle assessment (LCA). These are selective sulfidation with and without feed pretreatments, each with and without carbothermically-driven sulfur reflux (CDSR). For selective sulfidation and physical separation without pretreatment, the following process blocks are employed: nitrogen separation from air for sulfidation carrier gas production, sulfidation in a multihearth fluidized bed reactor, comminution, physical separation via froth flotation, and waste gas stream handling via a cyclone separator, followed by either electrostatic solids precipitator and dual alkali scrubbing (when the carbothermically-driven sulfur reflux, CDSR, is utilized in sulfidation) or sulfuric acid production (No CDSR). Materials containing impurities such as normally occurring radioactive elements or anions other than oxygen and sulfur may require additional pretreatments prior to selective sulfidation. The environmental impacts

of selective sulfidation with some possible material feed preparation / pretreatment steps are also considered, such as feed drying, calcination for defluorination of fluorocarbonate minerals or lithium ion battery electrolytes and oxidation of mixed metal compounds such as rare earth magnets, sulfidation for dephosphorization of phosphate minerals and dethoriation of rare earth concentrates, and sulfidation/calcination for sintering of material feeds too finely ground for effective liberation and physical separation of sulfide precipitants post selective sulfidation. Process flow diagrams are included in Figures E8 and S1-S3. Operating conditions are included in Tables S16-S17.

For these scenarios, three representative sulfidation feedstock chemistries are considered: copper(I) oxide (Cu_2O), nickel(II) oxide (NiO), and neodymium(III) oxide (Nd_2O_3). System boundaries consisting of an input of feed and an output of processed feed for each of the four generic processes are included in Figures E8 and S1-S3. The impacts of flows originating within the system boundary are evaluated from the cradle through usage in the process, while the impacts of flows originating outside the system boundary are evaluated from the system gate through usage in the process. Environmental impact categories of global warming potential (GWP), terrestrial acidification (TA), and water resource depletion (WRD) are adopted. A functional unit of 1 kg of selective sulfidation feed is chosen, enabling the avoidance of allocation of environmental impacts between coproducts in accordance with ISO 14040[89]. Impacts may be reallocated per unit of product if the product grade and recovery fraction are known, with allocation conducted via ISO 14040 hierarchy[89]: (1) Partition of processes steps into sub-processes to isolate the impacts of individual coproduct. (2) Allocation of impacts between coproducts based on physical relationships, such as mass fraction. (3) Allocation of impacts between coproducts based on non-physical relationships, such as economic value.

To compare environmental impacts of material processing via selective sulfidation versus nonselective pyrometallurgy with selective hydrometallurgy, three materials-specific case studies are chosen: Zirconium-silicon separation from zircon, iron-titanium separation from ilmenite, and rare earth element separation from bastnaesite. These case studies are selected for two reasons: 1 – the existing processes – alkali fusion, the sulfate process, and acid roasting/leaching/solvent extraction respectively – each involve a combination of non-selective pyrometallurgical and selective hydrometallurgical treatments, serving to elucidate the possible environmental impact reduction by increasing the selectivity of pyrometallurgical processing steps using sulfidation chemistry. 2 – each of these processes has well-established feedstocks, LCA data, system boundaries, and allocation strategies for the standard processing route, supporting fair comparison of impacts between selective sulfidation with physical separation and hydrometallurgical chemical separation.

The environmental impact of zirconium oxide and silicon oxide separation from zircon is compared between the standard alkali fusion process and selective sulfidation using LCA. Environmental impact data for alkali fusion is available in a published study[49]. System boundaries for selective sulfidation are defined to be an input of zircon, and an output of silicon and mixed zirconium-hafnium oxide as shown in Figure S7. A functional unit of 1 kg of zirconium oxide is adopted for the impact categories of GWP, TA, and WRD. Division of environmental impacts between coproducts is conducted via the ISO 14040[89] hierarchy. Allocation of impacts between zirconium and hafnium product oxides are conducted a mass basis, as described in Table S25. The same allocation fractions are adopted herein as those for the published study[49] on the alkali fusion process, supporting equitable comparison of impacts between the pathways.

The environmental impact of iron-titanium oxide separation from ilmenite is compared between the standard sulfate process and selective sulfidation using life cycle assessment. LCA impact data for the sulfate process is available in a published study[49]. System boundaries for selective sulfidation are defined to be an input of ilmenite, and an output of titanium dioxide and iron sulfide, as shown in Figure S8. A functional unit of 1 kg of titanium dioxide is adopted for the impact categories of GWP, TA, and WRD. As for the published LCA of the sulfate

process[49], environmental impacts are fully attributed to titanium dioxide production, supporting equitable comparison of impacts between the two pathways and eliminating the need for environmental impact allocation.

The environmental impact of rare earth element separation from bastnaesite, the most commercially-relevant source of light rare earth elements, is compared between the standard acid roasting, leaching, and solvent extraction pathway and selective sulfidation using LCA. Environmental impact data for the standard hydrometallurgical route is available in a published study[9]. System boundaries for selective sulfidation are defined to be an input of pre-concentrated (non-defluorinated, non-dethoriated) bastnaesite rare earth fluorocarbonate, and an output of separated rare earth element compounds as shown in Figures S9-S10, hypothetically processed at the world's largest rare earth element producer at the Bayan Obo facility in China. A functional unit of 1 kg of separated rare earth elements is adopted for the impact categories of GWP, TA, and WRD. To avoid the need for allocation of environmental impacts between rare earth coproducts as recommended by ISO 14040[89], environmental impacts are reported on the basis of total mass of separated rare earth oxide. This eliminates the need for allocation of environmental impact between rare earth oxide by- and coproducts, and supports fair comparison of environmental impacts to the published study[9] detailing the hydrometallurgical route, which also reports impacts for a functional unit of 1 kg of total separated rare earth oxides. Allocation data is reported in Table S25.

Inventory Analysis

For determinization of environmental impacts for the four generic sulfidation processes, process flow diagrams with system boundaries are depicted in Figures E8 and S1-S3. For these processes, a functional unit of 1 kg of selective sulfidation feed is adopted. When product feed grade and recovery are known, impacts may be reallocated to the product itself. Baseline, lower bound, and upper bound operating conditions for the generic processes are reported in Tables S16-S17. For the case studies of zirconium-silicon, iron-titanium, and rare earth element separations via selective sulfidation, process flow diagrams are included in Figures S7-S10, with operating conditions reported in Tables S19-S21. For estimation of the predicted environmental impacts of separation via selective sulfidation, the following assumptions are made:

- The substitution of a selective sulfidation process for an existing process does not result in any major upstream (mining and beneficiation), downstream process (oxide reduction to metal) or product feedstock chemistry changes.
- For zirconium-silicon, iron-titanium, and rare earth element separations, new byproducts produced via selective sulfidation that are not present in the established process (sulfuric acid or metal compounds previously lost to waste) are presently not considered as allocable coproducts for environmental impacts. While they may be marketable byproducts, this is to support fair comparison of environmental impacts for selective sulfidation with the existing process.
- Comminution for product liberation following sulfidation is taken to have similar technosphere inputs as for high intensity stirred milling in conventional sulfide ore beneficiation.
- Physical separation of products via froth flotation following sulfidation is taken to have similar technosphere inputs as for conventional sulfide ore beneficiation.
- For the generic, zirconium-silicon, and titanium-iron selective sulfidation processes the environmental impacts associated with electricity, heat, and reagent production are taken from global average inventory data, as available through the ecoinvent 3.6 database. Natural gas combustion is assumed for heat production, with emissions as reported by the United States Environmental Protection Agency. Electricity production (high voltage) is assumed to occur via natural gas combustion at a combined cycle power plant, with global average data from ecoinvent 3.6 employed.

- For rare earth element separation, the environmental impacts associated with electricity, heat, reagent production, and transportation are assumed to be that reported for the Inner Mongolia region of China, as available through the ecoinvent 3.6 database. For inputs where data for the Inner Mongolia region is unavailable, China national average data from the ecoinvent 3.6 database is employed. For inputs where data is unavailable for Inner Mongolia or China as a whole, global average data as available through the ecoinvent 3.6 database is utilized. Natural gas combustion is assumed for heat production, with emissions as reported by the United States Environmental Protection Agency. Electricity production via heavy fuel oil combustion in Inner Mongolia is assumed as reported in the ecoinvent 3.6 database.
- Environmental impacts associated with feedstock transportation are excluded for the generic, zirconium-silicon, and titanium-iron selective sulfidation processes. Transportation is also excluded in the published LCA[49] for zirconium-silicon separation via alkali fusion and titanium-iron separation via the sulfate process, supporting fair comparison.
- Reagent transportation requirements are assumed to be equivalent for rare earth element separation via selective sulfidation and the conventional pathway, as reported in the published hydrometallurgical study[9].
- Nitrogen carrier gas, sulfur, and carbon utilization are informed by the experimental results presented herein. Carrier gas is recycled at a rate of 90%, corresponding to a purge fraction of 10%. When CDSR is employed, carbon monoxide in the purge stream is combusted to carbon dioxide, with no heat recovered.
- The stepwise order of metal separation is taken to follow the sulfidation series presented in Figure 1a. In practice metal removal could be performed for the most prevalent metals first by employing parallel sulfidation reaction pathways, reducing energy consumption from material heating.
- SO_2 produced in sulfidation and calcination reactions is recovered for sulfuric acid production at a rate of 99%, on par with modern sulfuric acid production efficiencies as reported in ecoinvent 3.6.
- In conventional sulfuric acid production, some electricity is generated from steam produced during sulfur combustion to SO_2[88]. Since SO_2 is produced as a biproduct of the sulfidation reaction and not from direct sulfur combustion, this electricity generation is excluded in the present analysis.
- In conventional sulfuric acid production, some electricity is generated from hot acid heat recovery systems[88]. This electricity generation is included in the present analysis to partially offset electricity needs in selective sulfidation and physical separation.
- The environmental impacts associate with offsite solid and liquid waste processing are presently not considered for selective sulfidation. Likewise, the are also not considered in the published studies[9,49] of zirconium-silicon, iron-titanium, and rare earth elements separation from bastnaesite via the conventional process.
- Contributions to environmental impact from facilities construction and infrastructure are excluded, as in the published study[9] for rare earth elements separation via the conventional process.
- For selective sulfidation, each element separated is taken to require its own selective sulfidation and physical separation circuits.
- Initial removal of fluorine from bastnaesite is accomplished via sodium carbonate roasting and subsequent washing with water.
- Soda ash consumption is assumed to be stoichiometric for defluorination of bastnaesite.
- The sulfidative sintering process in rare earth element processing is predicted to be autothermal, as observed for conventional industrial roasting processes.

- The thermodynamics of mixed rare earth oxide and rare earth mineral gangue are taken to be well represented by those for neodymium oxide and iron oxide respectively.
- Error bars in the environmental impacts for the generic sulfidation processes are taken to be +/- two standard deviations as determined via Monte Carlo simulation. Baseline, lower bound, and upper bound operating conditions are reported in Tables S16-S17. Error is discussed in greater detail below in *Sensitivity Analysis*.
- Error bars for the environmental impact of zirconium-silicon, titanium-iron, and rare earth element separation via selective sulfidation are taken to be an equivalent percentage above and below the mean as determined through Monte Carlo simulation of the relevant generic case. Error is discussed in greater detail below in *Sensitivity Analysis*.

While such assumptions may seem academic, they establish a framework that supports quantifiable determination of a life cycle inventory for selective sulfidation as it could possibly be applied at an industrial scale. Energy inputs for pyrometallurgical reactions are calculated using FactSage 8.0, with a summary of relevant thermodynamic data included in Table S27-S31. The environmental impacts of electricity, process heat, and reagent generation, production, and usage are compiled from ecoinvent 3.6 data for relevant locations as described in the above assumptions. The net material and energy balance for production of zirconium oxide production from zircon, titanium dioxide from ilmenite, and separated rare earth oxides from bastnaesite concentrate as processed via selective sulfidation are presented as the life cycle inventories (LCI) in Tables S22-S24. Impact assessment and sensitivity analysis for these LCI's are described in the following sections.

Impact Assessment

In the previous section, we motivate and present a lifecycle inventory (LCI) for production of zirconium oxide from zircon, titanium dioxide from ilmenite, and pure rare earth oxides from bastnaesite concentrate via hypothetical pyrometallurgical selective sulfidation processes.

We use these LCI's to explore the possible environmental impacts of selective sulfidation and compare those impacts in the categories of global warming potential (GWP), terrestrial acidification (TA), and water resource depletion (WRD) to conventional processes that employ a series of nonselective pyrometallurgical and selective hydrometallurgical steps. These impact categories are selected due to their straightforward determination from presumed process-scale and thermodynamic data available for and pertinent to a hypothetical selective sulfidation process. However, many other environmental impact categories exist, including but not limited to ozone depletion, eutrophication, particle emissions, ecotoxicity, and mineral resource depletion, which need to be considered to fully understand the environmental sustainability of a hypothetical selective sulfidation process.

In general, comparison and scaling of multiple industrial ecology studies can be difficult due to different underlying assumptions and allocations that necessitate the need for data harmonization[7]. To avoid the need for extensive data harmonization, we selected materials separation and production case studies for two reasons: 1 – the existing processes – alkali fusion, the sulfate process, and acid roasting/leaching/solvent extraction respectively – each involve a combination of non-selective pyrometallurgical and selective hydrometallurgical treatments, serving to elucidate the possible environmental impact reduction by increasing the selectivity of pyrometallurgical processing steps using sulfidation chemistry. 2 – each of these processes has well-established feedstocks, LCA data, system boundaries, and allocation strategies for the standard processing route, supporting fair comparison of impacts between selective sulfidation with physical separation and hydrometallurgical chemical separation.

Energy, reagent, water and emission data for selective sulfidation are compiled using mass balances, energy balances, and published unit operation data, supplemented as required with data from ecoinvent 3.6[90]. GWP and TA are quantified over the system boundaries (Figure

E8, S1-S3, and S7-S10) using the Tool for Reduction and Assessment of Chemicals and Other Environmental Impacts (TRACI 2.1)[94]. Water resource depletion is tabulated following the methodology employed in the published LCA for rare earth element separation via the conventional processing pathway[9].

Distributions of GWP, TA, and WRD produced via Monte Carlo simulation of the generic process (Figures E8 and S1-S3) are depicted in Figure E10. For a generic sulfidation process without carbothermically-driven sulfur reflux (CDSR), the global warming potential (GWP), terrestrial acidification (TA), and water resource depletion (WRD) are estimated to be on the order of 0.20 (+/- 0.06) kg CO_2-eq, $9x10^{-3}$ (+/- $5x10^{-3}$) kg of SO_2-eq, and 9 (+/- 4) kg H_2O respectively per kg of feed, presented in Figure E10. The inclusion of pretreatments such as feed drying, calcination/roasting, and sintering on average increase GWP by about 50%, WRD by 30% and TA by double over the base case, as tabulated in Table S18. The use of CDSR in selective sulfidation meanwhile increases GWP by a factor of 4-5x and WRD by a factor of 3-4x. Trends are discussed in the following section, *Interpretation*. Clearly, the sustainability of every materials separation challenge is influenced differently by feedstock chemistry, grade, and purity, motivating materials-specific case studies. The GWP, TA, and WRD of zirconium oxide production via zirconium-silicon separation from zircon are predicted to be on the order of 0.12 kg CO_2-eq, 0.02 kg SO_2-eq, and 15 kg H_2O respectively (Table S26), all per kg of ZrO_2. The GWP, TA, and WRD of titanium dioxide production via titanium-iron separation from ilmenite are predicted to be on the order of 0.53 kg CO_2-eq, 0.01 kg SO_2-eq, and 18 kg H_2O respectively (Table S26), all per kg of TiO_2. Finally, the GWP, TA, and WRD of rare earth element separation from bastnaesite are predicted to be on the order of 8.1 kg CO_2-eq, 0.09 kg SO_2-eq, and 79 kg H_2O respectively (Table S26), all per kg of separated rare earth oxide. These impacts may be broken down into contributions from defluorination, dethoriation, rare earth element separation, and reagent transportation, included in Table S27. Comparison of the predicted environmental impacts of selective sulfidation to that of existing processes are discussed in the following section.

Interpretation

Predicted environmental impacts for the generic sulfidation case study serve as a first pass estimate for the environmental impact of a selective sulfidation process. However, the values reported in Figure E10 and Table S18 do not substitute for chemistry and process-specific analysis. Of note, the bimodal nature of the GWP distribution is due to differences in oxygen content of the three model chemistries considered in the Monte Carlo simulation, highlighting the role of system chemistry in determining environmental impact. The generic process also makes no distinction between adding selective sulfidation as a pretreatment at an established facility versus conducting selective sulfidation at a greenfield project. This distinction is particularly important with regards to the use of selective sulfidation during mineral processing and beneficiation. Comminution can dominate the energy usage and GWP of beneficiation steps[10], so care must be taken to avoid over or undercounting the environmental impact of comminution when contextualizing the environmental impacts of the generic selective sulfidation process.

For selective sulfidation processes without CDSR, the largest sources of GWP are electricity usage in comminution and air separation for nitrogen carrier gas production. When CDSR is employed, direct CO_2 emissions increase GWP, as shown in Figure E10. The decarbonization of electricity production is one avenue to lower the GWP of selective sulfidation. Likewise, the use of CDSR for process control should be avoided when possible. Acidification is largely the result of imperfect conversion of SO_2 to sulfuric acid, with the use of CDSR lowering terrestrial acidification. The other major contributor to acidification is elemental sulfur production, with smaller contributions from

power generation and fuel combustion. WRD is mostly driven by cooling water loss to steam during cryogenic air separation, with some water resource depletion also occurring during electricity generation, physical separation via froth flotation, reagent production, and acid production.

Selective sulfidation with physical separation is predicted to reduce the GWP of hydrometallurgical zirconium-silicon and titanium-iron separations[49] by over 80% each (Figure 3b). Meanwhile, selective sulfidation with CDSR and physical separation is predicted to show reductions to GWP of 60-90%, TA of over 70%, and WU of 65-85% for rare earth separation versus conventional[9] hydrometallurgical processing of bastnaesite via acid roasting, leaching, and solvent extraction (Figure 3b). These reductions to environmental impacts are not a surprise. Presently, zirconium oxide production from zircon via alkaline fusion, titanium dioxide production from ilmenite via the sulfate process, and rare earth separation from bastnaesite via acid roasting, leaching, and solvent extraction all require a series of nonselective pyrometallurgical pretreatments followed selective hydrometallurgical processes. When the selectivity of these pyrometallurgical steps can be increased through the use of sulfidation chemistry, the complexity and number of hydrometallurgical treatments required downstream may be reduced, thereby lowering the environmental impact of the process. Selective sulfidation is likewise promising alternative for nonselective pyrometallurgical processes that rely on subsequent hydrometallurgy for selective product recovery, such as pyrometallurgical lithium ion battery recycling. Overall, our experimental findings indicate that elements previously requiring a series of harsh pyrometallurgical and hydrometallurgical separations can now be isolated through a single, pyrometallurgical sulfidation step that supports simple and conventional physical separation technologies. Our life cycle assessment results indicate that when pyrometallurgical methods are sufficiently selective to minimize the need for subsequent hydrometallurgical treatments, as demonstrated herein using selective sulfidation, the environmental impact of materials processing may be lowered. Monte Carlo simulation illustrates that this conclusion is resilient to uncertainties surrounding operating conditions, as we discuss in the following section, *Sensitivity Analysis.*

Sensitivity Analysis

Sensitivity analysis for the environmental impacts of the generic sulfidation processes are conducted via Monte Carlo simulation. For each of the four generic processes 360,000 iterations were conducted over process parameters as shown in Tables S16-S17. Thermodynamic inputs for mass and energy balances were randomly varied using coupled discrete, uniform distributions across the sulfidation chemistries of copper (Cu_2O), neodymium (Nd_2O_3), and nickel oxides (NiO) each with and without employment of CDSR. Operating conditions were varied using continuous triangular distributions. When uninformed by literature, upper and lower bounds for triangular distributions were taken as -50% to +100% of the base value[76]. Distributions for GWP, TA, and WRD for each generic sulfidation process are included in Figure E10.

Sensitivity analysis via Monte Carlo simulation reveals that the largest source of uncertainly in the GWP of selective sulfidation is whether or not CDSR is employed in the process. Meanwhile, for WRD, the largest source of uncertainty is whether or not feed pretreatments are required. Specifically, the need for sulfidative sintering increases the amount of nitrogen carrier gas employed, thereby increasing WRD associated with air separation. For TA, uncertainty is shared between process operating conditions, the use of pretreatments, and the use of CDSR.

For a given generic selective sulfidation process, the largest sources of uncertainty for environmental impacts per mass of feed are the feedstock chemistry and sulfidation conversion. Differences in compound molar mass and stoichiometry lead to large variations in the amount of anion oxygen that can be exchanged with sulfur. Differences in chemistry change not only the oxygen content of the feed, but also the amount of external heating required for the reactor to remain at temperature. Variations in conversion likewise are responsible for differences in the amount of anion oxygen that can be exchanged with sulfur, and thereby the exothermicity of the sulfidation reaction. Heating requirements are also

affected by the efficiency of waste heat recovery in the thermal recuperator, although uncertainty in this parameter is often outweighed by those in chemistry and conversion, which themselves lead to bimodal distributions in GWP. Variation in WRD is tied almost exclusively to variation in cooling water usage, which largely outweighs water lost in froth flotation and utilized in acid and reagent production. TA is almost directly related to conversion and chemistry, and exhibits wide error distributions with respect to its mean.

Experimental results herein inform whether feed pretreatments or CDSR are required for a process, leaving operating chemistry and conditions as the main source of uncertainty for a materials-specific case study. For error analysis in the material specific case studies for zirconium-silicon, titanium-iron, and rare earth separations, error bars are determined from Monte Carlo simulation of the relevant generic process (with or without pretreatment, with or without CDSR). Error bars for GWP, WRD, and TA corresponding to +/- two standard deviations as a percentage of the generic case study mean are employed for environmental impacts for zirconium-silicon, titanium-iron, and rare earth separations. Since feed chemistry is the largest contributor to the error in the environmental impact of selective sulfidation, and chemistry is a known factor for each of these case studies, this methodology likely overestimates the error of each materials specific process. Nevertheless, the improvements to environmental impact afforded by selective sulfidation remain resilient to these uncertainties.

Supporting Code and Files for the Technoeconomic Analysis and Life Cycle Assessments

Below are descriptions of the files and code used for the technoeconomic analysis (TEA) and life cycle assessments (LCA) of selective sulfidation of metal compounds. Files and code are available for download at https://doi.org/10.7910/DVN/193PW2 [96] or from the authors upon request. The MATLAB code that compiles and runs the Monte Carlo simulation is set up to run on 6 computer cores in parallel to reduce computation time. The code is written for MATLAB R2021a, and requires the "Parallel Computing" and "Statistics and Machine Learning" Toolboxes. Key files and code are identified as follows, where XXX denotes multiple files of similar function:

- MC_compiler.m : Executing this MATLAB script will run the Monte Carlo Simulations for the TEA and LCA in their entirety. On a Windows 10 machine utilizing an Intel i7-9700 CPU, 500GB solid state hard drive, 16GB of RAM, and NVIDIA GeForce GTX 1660 Ti graphics card, this takes around 24-48 hours to complete.
- OPEX_MC_XXX.m : Executing one of these MATLAB scripts will run the Monte Carlo Simulation for mass and energy balances and economic data for the given scenario. Input conditions and results are tabulated in OPEX_MC_XXX.xlsx. Mass and energy balances and economic data are calculated in the Cu2O_XXX.xlsx, NiO_XXX.xlsx, and Nd2O3_XXX.xlsx spreadsheets. Variable distributions are determined, input into the calculation spreadsheet, and results extracted using MC_XXX.m scripts. On a Windows 10 machine utilizing an Intel i7-9700 CPU, 500GB solid state hard drive, 16GB of RAM, and NVIDIA GeForce GTX 1660 Ti graphics card, each of these scripts took around 6-12 hours to complete.
- OPEX_MC_XXX.xlsx : Spreadsheet containing input parameters for variable distributions and output mass and energy balance and economic results of the Monte Carlo Simulation. OPEX_MC_XXX.xlsx files as provided have the results prepopulated, so it is not necessary to run MC_compiler.m or OPEX_MC_XXX.m scripts in order to extract results with MC_Analysis.m.
- Cu2O_XXX.xlsx : Spreadsheet used to calculate mass and energy balances and economic data for the copper oxide system chemistry. 6 equivalent files exist for each scenario (with and without pretreatment, with and without carbon) so that Monte Carlo simulation can be run on 6 computer cores in parallel. Results from each core and process chemistry are reaggregated in OPEX_MC_XXX.xlsx using OPEX_MC_XXX.m.

- NiO_XXX.xlsx : Spreadsheet used to calculate mass and energy balances and economic data for the nickel oxide system chemistry. 6 equivalent files exist for each scenario (with and without pretreatment, with and without carbon) so that Monte Carlo simulation can be run on 6 computer cores in parallel. Results from each core and process chemistry are reaggregated in OPEX_MC_XXX.xlsx using OPEX_MC_XXX.m.
- Nd2O3_XXX.xlsx : Spreadsheet used to calculate mass and energy balances and economic data for the neodymium oxide system chemistry. 6 equivalent files exist for each scenario (with and without pretreatment, with and without carbon) so that Monte Carlo simulation can be run on 6 computer cores in parallel. Results from each core and process chemistry are reaggregated in OPEX_MC_XXX.xlsx using OPEX_MC_XXX.m.
- MC_XXX.m : Scripts that generate variable distributions for input into and reads the results from Cu2O_XXX.xlsx, NiO_XXX.xlsx, and Nd2O3_XXX.xlsx. 6 equivalent scripts exist for each scenario (with and without pretreatment, with and without carbon) and chemistry so that Monte Carlo simulation can be run on 6 computer cores in parallel.
- MC_Analysis.m: MATLAB script to calculate environmental impacts from the Monte Carlo results tabulated in OPEX_MC_XXX.xlsx. OPEX and CAPEX data are also tabulated. When all OPEX_MC_XXX.xlsx files are populated, MC_Analysis.m can be run without rerunning OPEX_MC_XXX.m scripts. RareEarth.xlsx is required for the rare earth bastnaesite LCA case study.
- RareEarth.xlsx : similar to Nd2O3_XXX.xlsx above, utilized for mass and energy balance calculations for bastnaesite selective sulfidation and physical separation.
- HydroMC.m : Script for Monte Carlo simulation of hydrometallurgical CAPEX. Variable bounds are extracted from HydroOPEX.xlsx.
- HydroOPEX.xlsx : Variable bounds for operating conditions and economic data used in Monte Carlo Simulation of hydrometallurgical processes.

Supplementary Figures

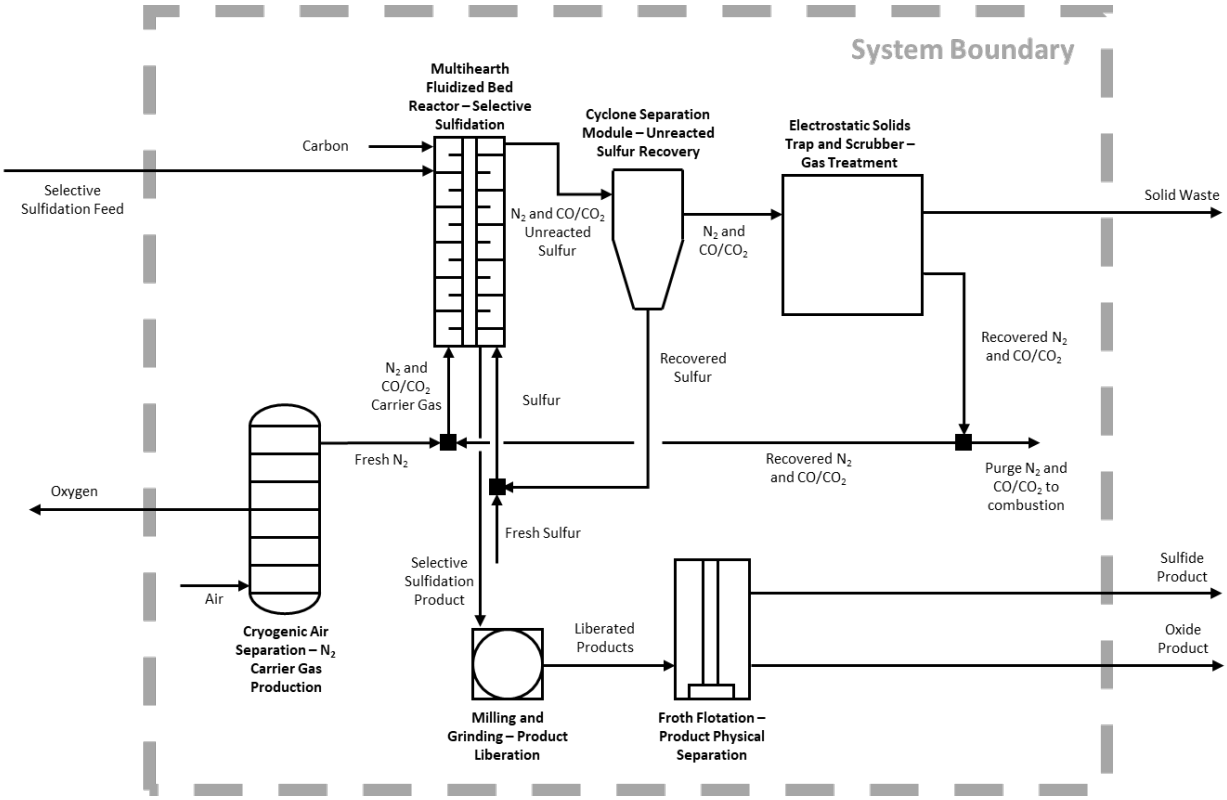

Figure S1: Flowsheet of a generic selective sulfidation process utilizing carbothermically-driven sulfur reflux (CDSR) for separation of an equimolar, mixed, binary oxide feed, consisting of air separation for nitrogen carrier gas production, selective sulfidation in a multihearth fluidized bed reactor, product comminution and physical separation via froth flotation, and downstream gas handling and treatment via a cyclone separator for solid particle removal and electrostatics solid trap and scrubber for SO_2 treatment.

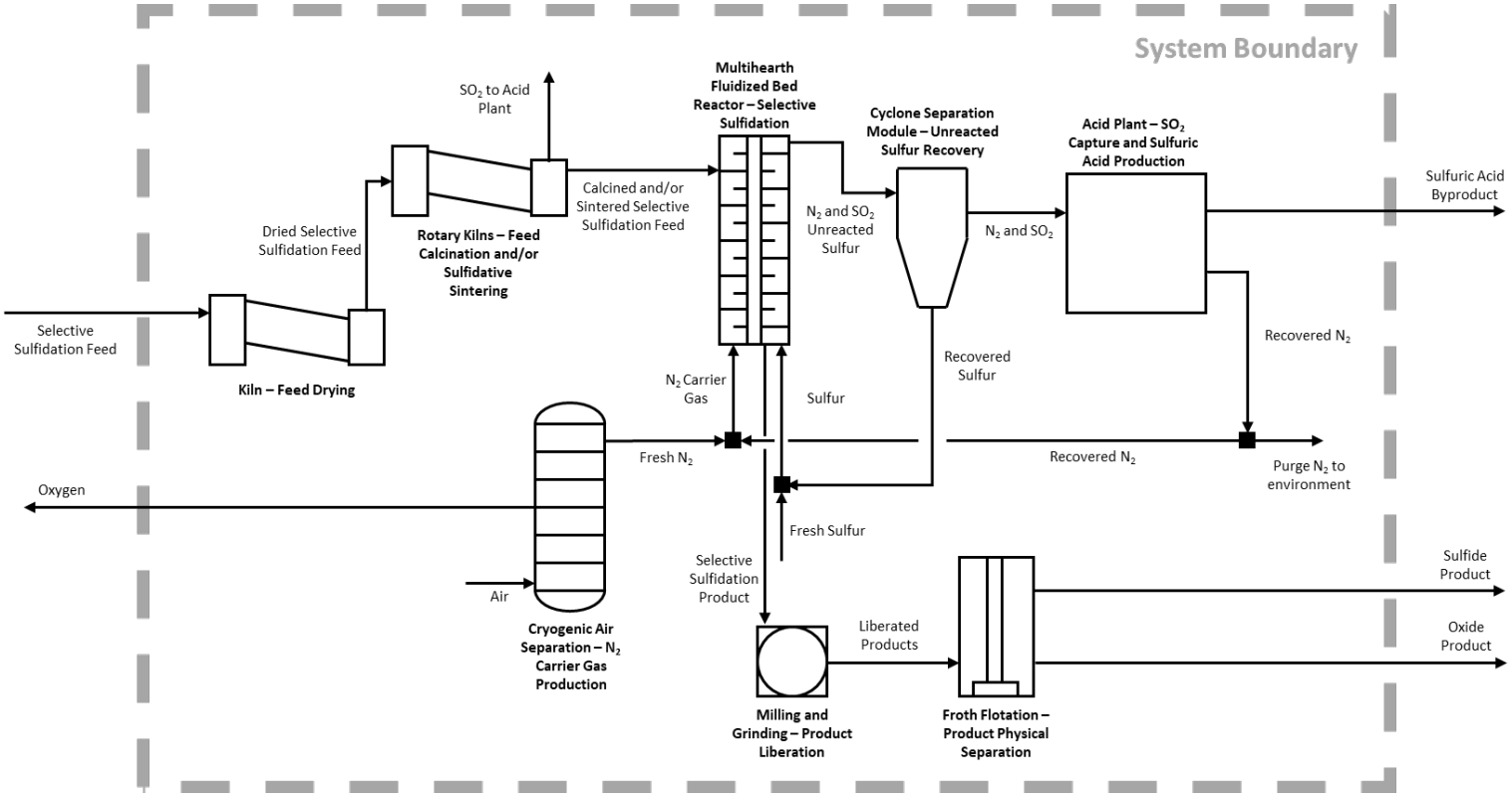

Figure S2: Flowsheet of a generic selective sulfidation process without carbothermically-driven sulfur reflux (CDSR) for separation of an equimolar, mixed, binary oxide feed, consisting of air separation for nitrogen carrier gas production, drying and sulfidation/calcination pretreatments, selective sulfidation in a multihearth fluidized bed reactor, product comminution and physical separation via froth flotation, and downstream gas handling and treatment via a cyclone separator for solid particle removal and acid plant for SO_2 recovery.

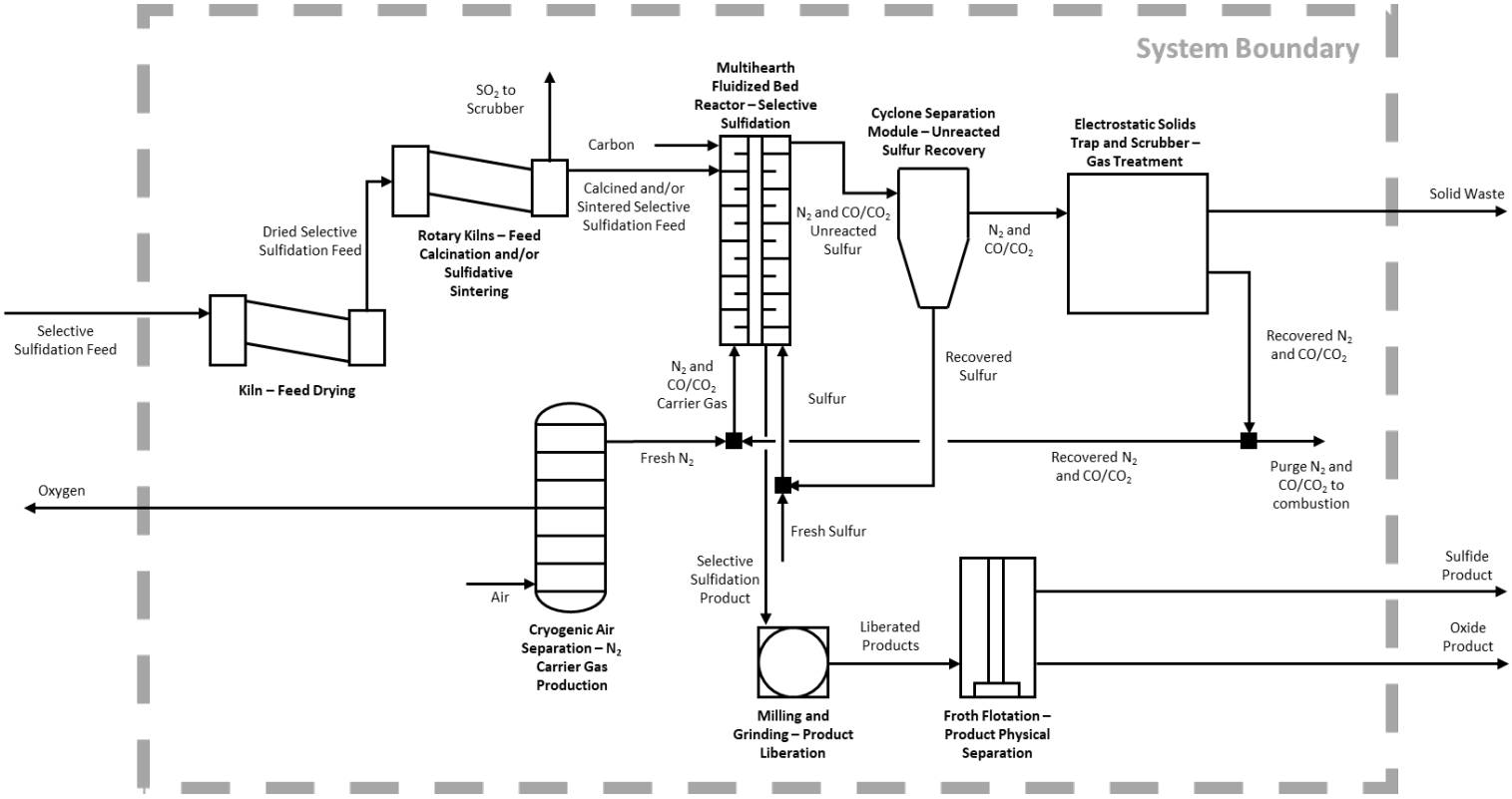

Figure S3: Flowsheet of a generic selective sulfidation process utilizing carbothermically-driven sulfur reflux (CDSR) for separation of an equimolar, mixed, binary oxide feed, consisting of air separation for nitrogen carrier gas production, drying and sulfidation/calcination pretreatments, selective sulfidation in a multihearth fluidized bed reactor, product comminution and physical separation via froth flotation, and downstream gas handling and treatment via a cyclone separator for solid particle removal and electrostatics solid trap and scrubber for SO_2 treatment.

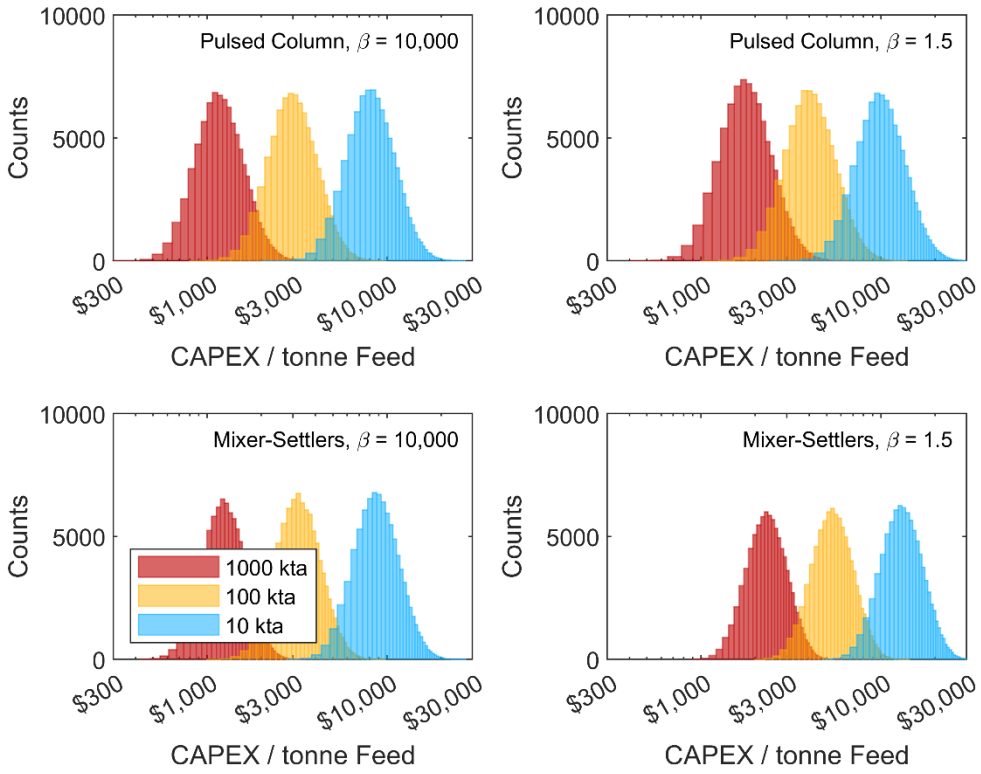

Figure S4: Capital cost (CAPEX) distributions for the generic hydrometallurgical separation process utilizing pulsed column or mixer-settler liquid-liquid contactors, at hydrometallurgical separation factors of 1.5 and 10,000 corresponding to f-block and d-block element separation respectively. Distributions are determined via Monte Carlo simulation, with probability distribution for CAPEX and operating condition parameters described in Tables S15. Consistent with conventional wisdom[8], at high separation factors, pulsed columns and mixer settlers are predicted to be capitally competitive, while at low separation factors, pulsed columns are predicted to be capitally favorable.

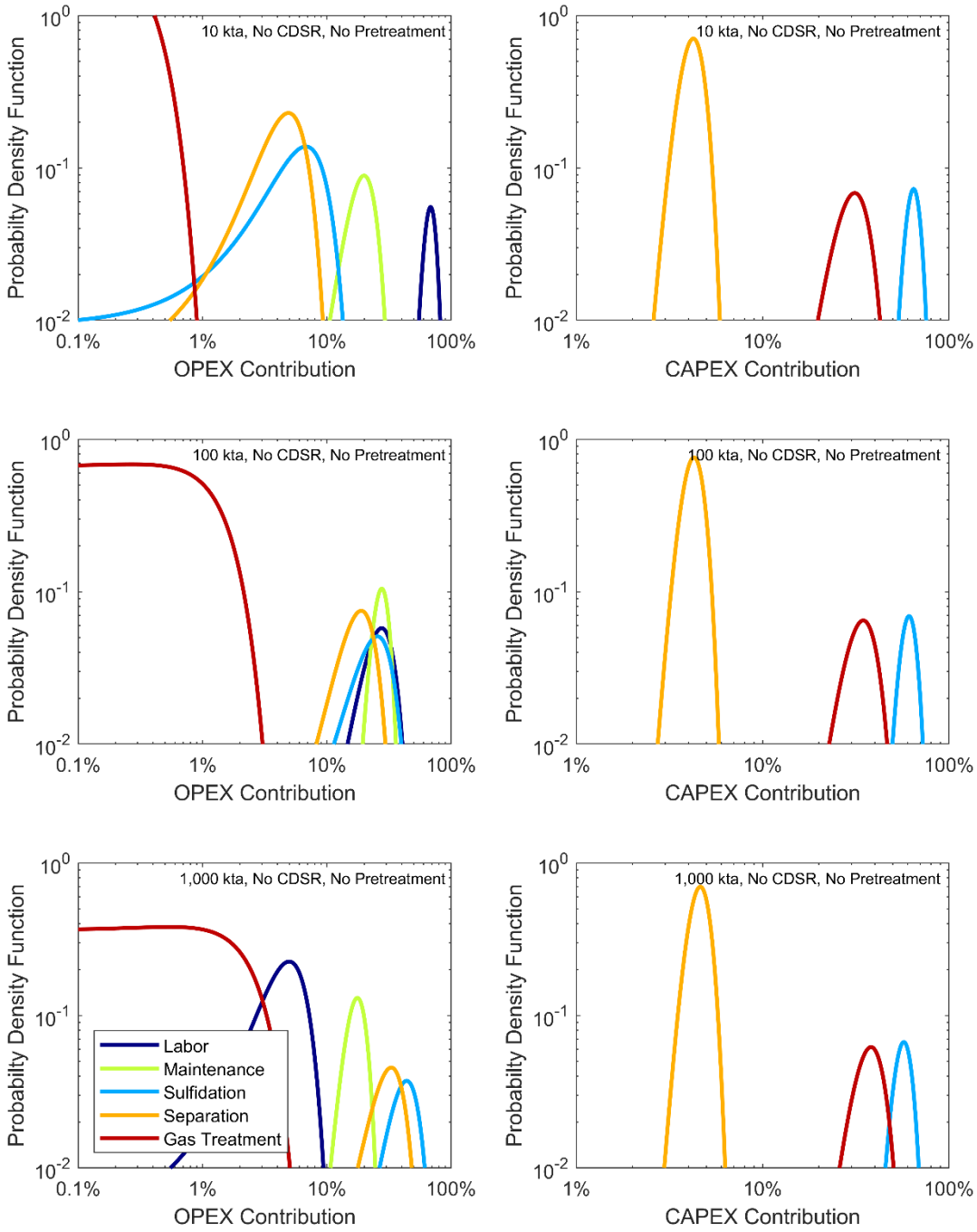

Figure S5: Probability distributions for percent contributions to CAPEX and OPEX for selective sulfidation without carbothermically-driven sulfur reflux (CDSR), corresponding to the flowsheet presented in Figure E8.

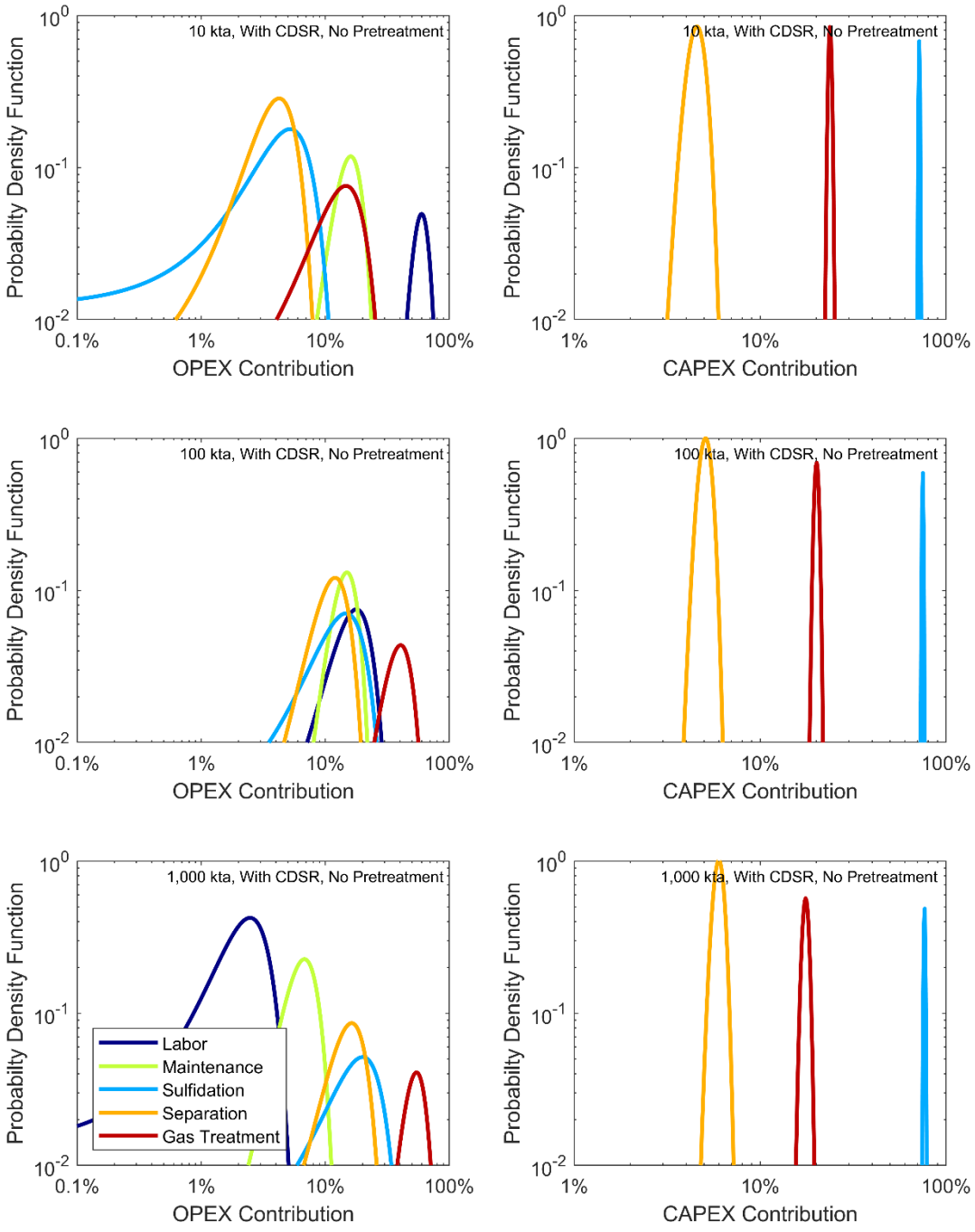

Figure S6: Probability distributions for percent contributions to CAPEX and OPEX for selective sulfidation with carbothermically-driven sulfur reflux (CDSR), corresponding to the flowsheet presented in Figure S1.

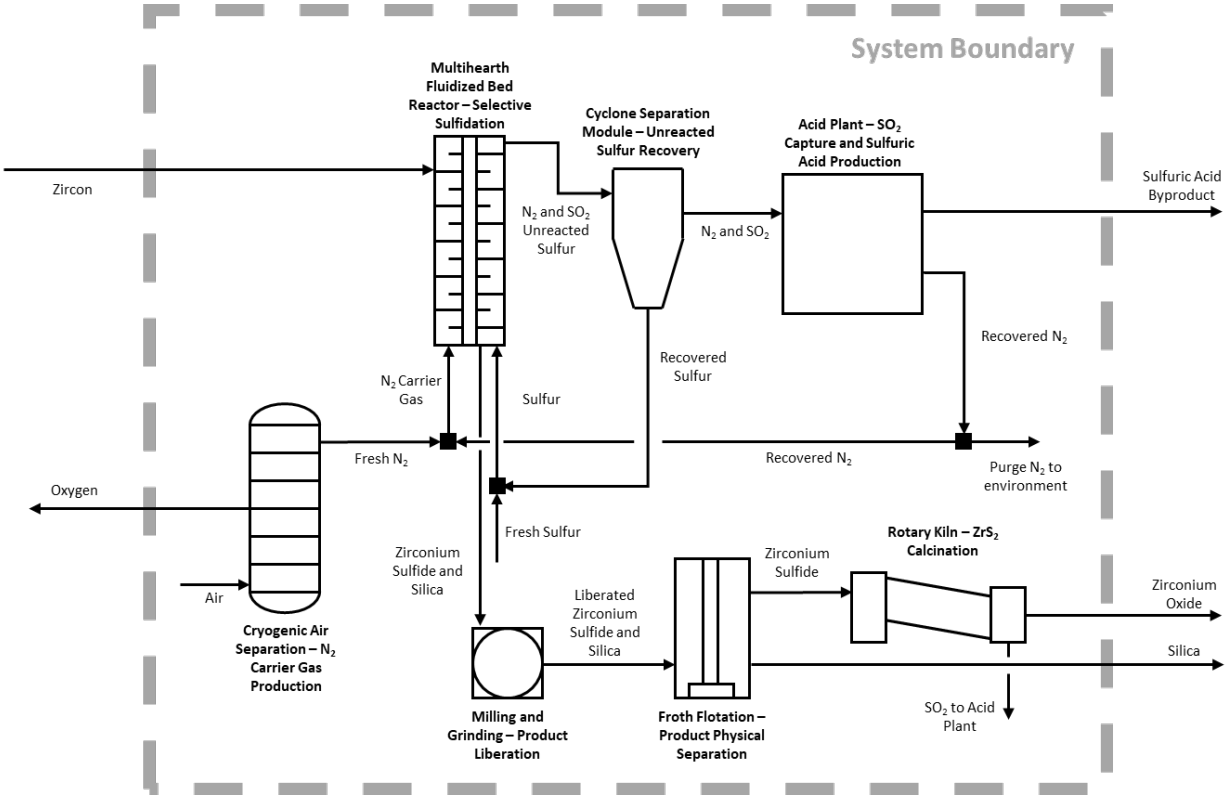

Figure S7: Flowsheet for zirconium oxide production via zirconium-silicon separation from zircon, consisting of air separation for nitrogen carrier gas production, selective sulfidation in a multihearth fluidized bed reactor, product comminution and physical separation via froth flotation, product calcination, and downstream gas handling and treatment via a cyclone separator for solid particle removal and acid plant for SO_2 recovery.

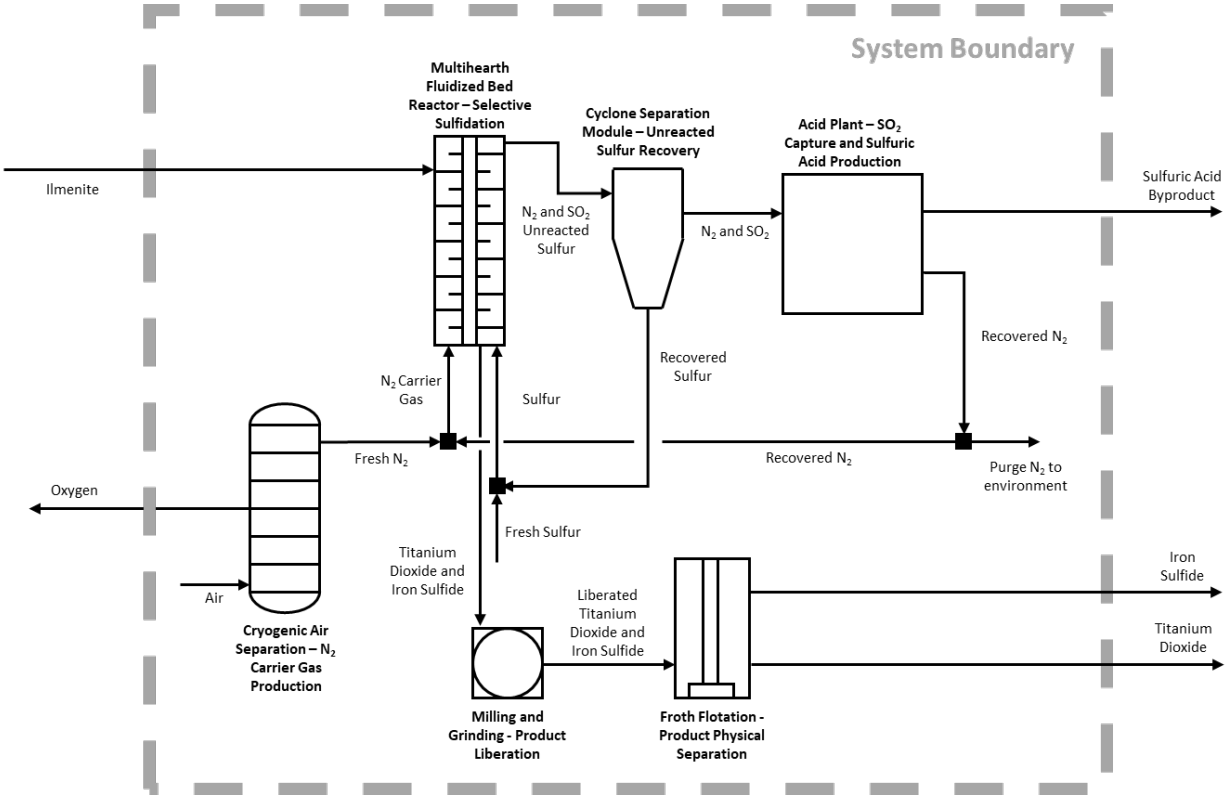

Figure S8: Flowsheet for titanium oxide production via titanium-iron separation from ilmenite, consisting of air separation for nitrogen carrier gas production, selective sulfidation in a multihearth fluidized bed reactor, product comminution and physical separation via froth flotation, and downstream gas handling and treatment via a cyclone separator for solid particle removal, and acid plant for SO_2 recovery.

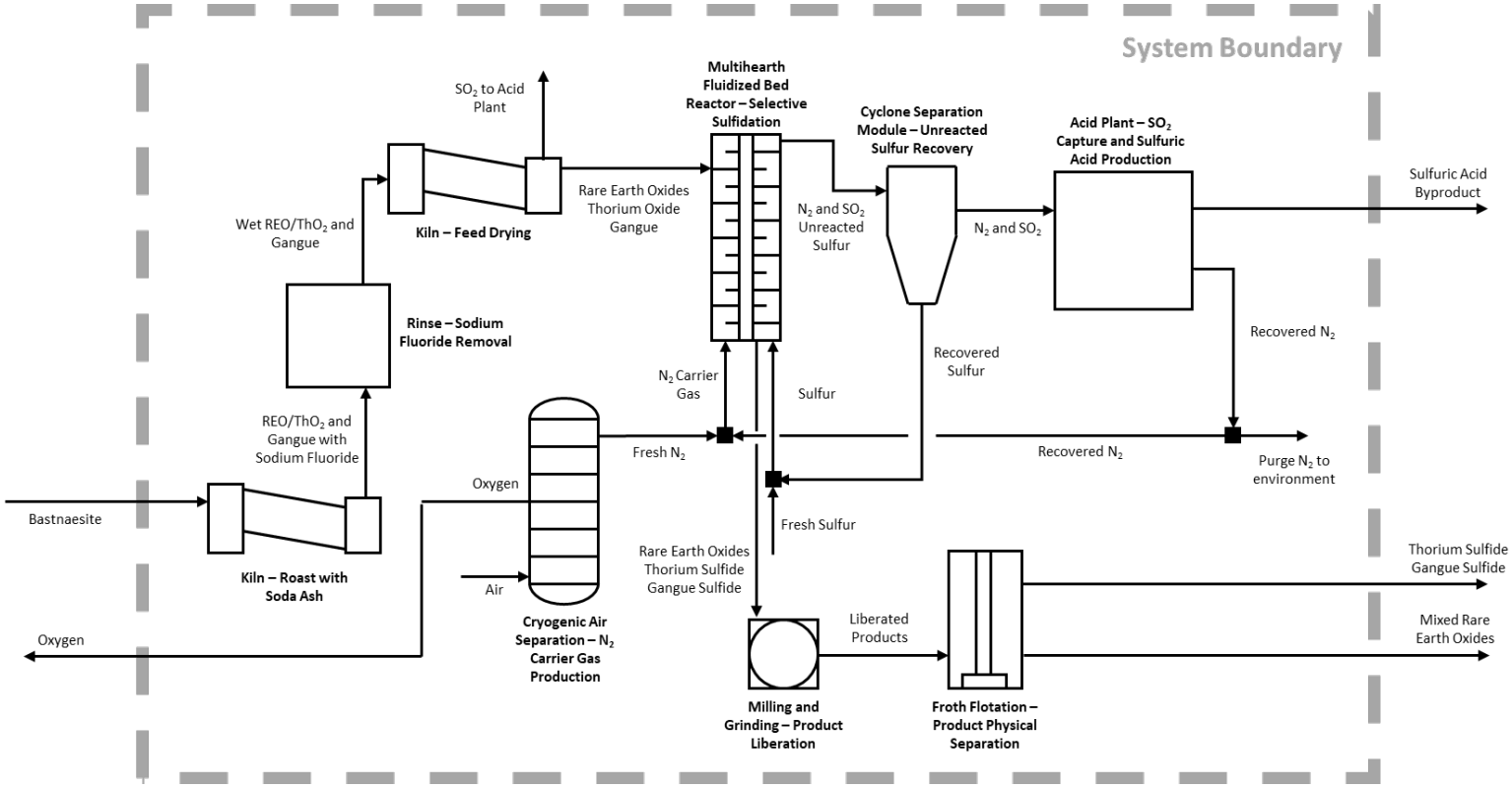

Figure S9: Flowsheet for bastnaesite defluorination and dethoriation to produce a mixed rare earth oxide, consisting of feed roasting with soda ash, feed rinsing, feed drying, air separation for nitrogen carrier gas production, selective sulfidation in a multihearth fluidized bed reactor, product comminution and physical separation via froth flotation, and downstream gas handling and treatment via a cyclone separator for solid particle removal and acid plant for SO_2 recovery.

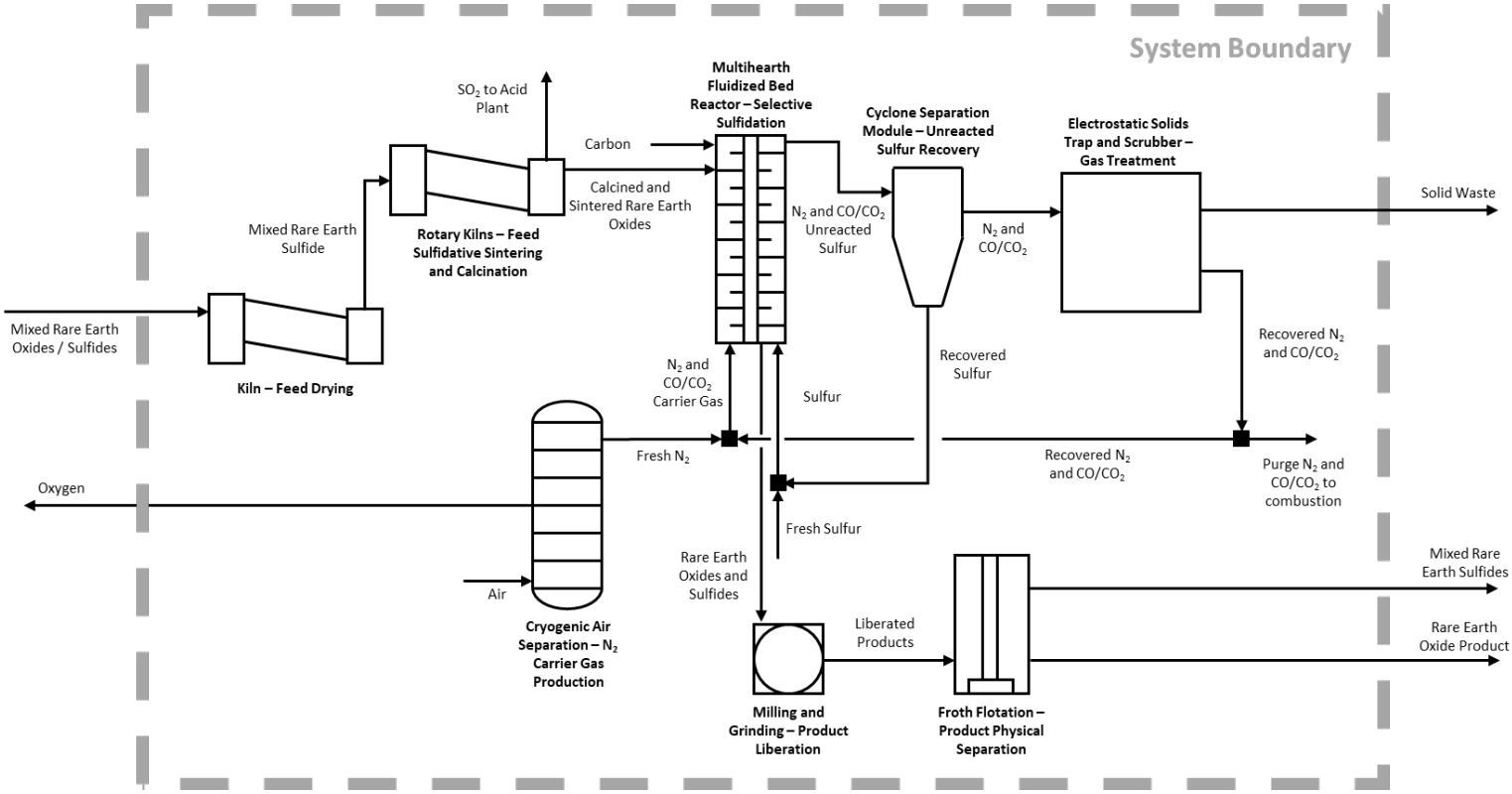

Figure S10: Flowsheet for rare earth oxide separation, consisting of feed drying, sulfidative sintering / calcination, air separation for nitrogen carrier gas production, selective sulfidation in a multihearth fluidized bed reactor utilizing carbothermically-driven sulfur reflux (CDSR), product comminution and physical separation via froth flotation, and downstream gas handling and treatment via a cyclone separator and electrostatics solid trap for solid particle removal, with a scrubber and acid plant for SO_2 treatment and recovery. This flowsheet may be repeated for each individual rare earth separation.

Full References (Same as for Main Text and Methods)

1. Cheisson, T. & Schelter, E. J. Rare earth elements: Mendeleev's bane, modern marvels. *Science (80-.).* **363**, 489–493 (2019).
2. Harper, G. *et al.* Recycling lithium-ion batteries from electric vehicles. *Nature* **575**, 75–86 (2019).
3. Enriquez, M. A. *et al.* Mineral supply for sustainable development requires resource governance. *Nature* **543**, 367–372 (2017).
4. Reck, B. K. & Graedel, T. E. Challenges in Metal Recycling. *Science (80-.).* **337**, 690–696 (2012).
5. Olivetti, E. A. & Cullen, J. M. Toward a sustainable materials system. *Science (80-.).* **360**, 1396–1398 (2018).
6. Ciez, R. E. & Whitacre, J. F. Examining different recycling processes for lithium-ion batteries. *Nat. Sustain.* **2**, 148–156 (2019).
7. K Lee, J. C. & Wen, Z. Pathways for greening the supply of rare earth elements in China. *Nat. Sustain.* **1**, 598–605 (2018).
8. Zhao, B., Zhang, J. & Schreiner, B. *Separation Hydrometallurgy of Rare Earth Elements*. (Springer International Publishing AG Switzerland, 2016).
9. Bailey, G. *et al.* Review and new life cycle assessment for rare earth production from bastnäsite, ion adsorption clays and lateritic monazite. *Resour. Conserv. Recycl.* **155**, 104675 (2020).
10. Norgate, T. & Jahanshahi, S. Low grade ores – Smelt, leach or concentrate? *Miner. Eng.* **23**, 65–73 (2010).
11. Yin, X. *et al.* Rare earth separations by selective borate crystallization. *Nat. Commun.* **8**, (2017).
12. Flytzani-Stephanopoulos, M., Sakbodin, M. & Wang, Z. Regenerative Adsorption and Removal of H2S from Hot Fuel Gas Streams by Rare Earth Oxides. *Science (80-.).* **312**, 1508–1510 (2006).
13. Valsamakis, I. & Flytzani-Stephanopoulos, M. Sulfur-tolerant lanthanide oxysulfide catalysts for the high-temperature water-gas shift reaction. *Appl. Catal. B Environ.* **106**, 255–263 (2011).
14. Pease, J. D., Curry, D. C. & Young, M. F. Designing flotation circuits for high fines recovery. *Miner. Eng.* **19**, 831–840 (2006).
15. Pease, J. D., Young, M. F., Curry, D. & Johnson, N. W. Improving fines recovery by grinding finer. *Trans. Institutions Min. Metall. Sect. C Miner. Process. Extr. Metall.* **119**, 216–222 (2010).
16. Han, J. *et al.* Effects of sodium salts on the sulfidation of lead smelting slag. *Miner. Eng.* **108**, 1–11 (2017).
17. Zhang, W., Zhou, Y., Zhu, J. & Pan, Y. New clean process for barium sulfide preparation by barite reduction with elemental sulfur. *Ind. Eng. Chem. Res.* **53**, 5646–5651 (2014).
18. Zhang, W. *et al.* Reaction mechanism study of new scheme using elemental sulfur for conversion of barite to barium sulfide. *Powder Technol.* **360**, 1348–1354 (2020).
19. Kaneko, T., Yashima, Y., Ahmadi, E., Natsui, S. & Suzuki, R. O. Synthesis of Sc sulfides by CS2 sulfurization. *J. Solid State Chem.* **285**, 121268 (2020).
20. Ahmadi, E. & Suzuki, R. O. An Innovative Process for Production of Ti Metal Powder via TiS x from TiN. *Metall. Mater. Trans. B* **51B**, 140–148 (2020).
21. Afanasiev, P. *et al.* Preparation of the mixed sulfide Nb2Mo3S10 catalyst from the mixed oxide precursor. *Catal. Letters* **64**, 59–63 (2000).
22. Ahmad, S., Rhamdhani, M. A., Pownceby, M. I. & Bruckard, W. J. Thermodynamic assessment and experimental study of sulphidation of ilmenite and chromite. *Trans. Institutions Min. Metall. Sect. C Miner. Process. Extr. Metall.* **123**, 165–177 (2014).
23. Harris, C. T., Peacey, J. G. & Pickles, C. A. Selective sulphidation and flotation of nickel from a nickeliferous laterite ore. *Miner. Eng.*

54, 21–31 (2013).

24. Liu, W., Zhu, L., Han, J., Jiao, F. & Qin, W. Sulfidation mechanism of ZnO roasted with pyrite. *Sci. Rep.* **8**, 9516 (2018).
25. Sohn, H. Y. & Fan, D.-Q. On the Initial Rate of Fluid-Solid Reactions. *Met. Mater. Trans. B* **48B**, 1827–1832 (2017).
26. Zagorac, D., Doll, K., Zagorac, J., Jordanov, D. & Matovic, B. Barium Sulfide under Pressure: Discovery of Metastable Polymorphs and Investigation of Electronic Properties on ab Initio Level. *Inorg. Chem.* **56**, 10644–10654 (2017).
27. Sohn, H. Y. & Kim, B.-S. A Novel Cyclic Process using CaSO 4 /CaS Pellets for Converting Sulfur Dioxide to Elemental Sulfur without Generating Secondary Pollutants: Part I. Feasibility and Kinetics of the Reduction of Sulfur Dioxide with Calcium-Sulfide Pellets. *Metall. Mater. Trans. B* **33B**, 711–716 (2002).
28. Sahu, S. K., Chmielowiec, B. & Allanore, A. Electrolytic Extraction of Copper, Molybdenum and Rhenium from Molten Sulfide Electrolyte. *Electrochim. Acta* **243**, 382–389 (2017).
29. Brown, A. M. & Ashby, M. F. Correlations for diffusion constants. *Acta Metall.* **28**, 1085–1101 (1980).
30. Nassar, N. T., Graedel, T. E. & Harper, E. M. By-product metals are technologically essential but have problematic supply. *Sci. Adv.* **1**, e1400180 (2015).
31. Olivetti, E. A., Ceder, G., Gaustad, G. G. & Fu, X. Lithium-Ion Battery Supply Chain Considerations: Analysis of Potential Bottlenecks in Critical Metals. *Joule* **1**, 229–243 (2017).
32. Dunn, J. B., Gaines, L., Sullivan, J. & Wang, M. Q. Impact of Recycling on Cradle-to-Gate Energy Consumption and Greenhouse Gas Emissions of Automotive Lithium-Ion Batteries. *Environ. Sci. Technol.* **46**, 12704–12710 (2012).
33. Shi, J. *et al.* Sulfation Roasting Mechanism for Spent Lithium-Ion Battery Metal Oxides Under SO2-O2-Ar Atmosphere. *JOM* **71**, 4473–4481 (2019).
34. Stinn, C. & Allanore, A. Selective Sulfidation and Electrowinning of Nickel and Cobalt for Lithium Ion Battery Recycling. in *Ni-Co 2021: The 5th International Symposium on Nickel and Cobalt* (eds. Anderson, C. et al.) 99–110 (Springer Nature Switzerland AG, 2021). doi:10.1007/978-3-030-65647-8_7
35. Wagner, M.-E. & Allanore, A. Chemical Thermodynamic Insights on Rare-Earth Magnet Sludge Recycling. *ISIJ Int.* **60**, 2339–2349 (2020).
36. Narayanan, R. P., Kazantzis, N. K. & Emmert, M. H. Selective Process Steps for the Recovery of Scandium from Jamaican Bauxite Residue (Red Mud). *ACS Sustain. Chem. Eng.* **6**, 1478–1488 (2018).
37. Jowitt, Si. M., Werner, T. T., Weng, Z. & Mudd, G. M. Recycling of the Rare Earth Elements. *Curr. Opin. Green Sustain. Chem.* **13**, 1–7 (2018).
38. Wang, J. & Hu, H. Selective extraction of rare earths and lithium from rare earth fluoride molten-salt electrolytic slag by sulfation. *Miner. Eng.* **160**, 106711 (2021).
39. Binnemans, K., Jones, P. T., Müller, T. & Yurramendi, L. Rare Earths and the Balance Problem: How to Deal with Changing Markets? *Journal of Sustainable Metallurgy* **4**, 126–146 (2018).
40. Firdaus, M., Rhamdhani, M. A., Durandet, Y., Rankin, W. J. & McGregor, K. Review of High-Temperature Recovery of Rare Earth (Nd/Dy) from Magnet Waste. *J. Sustain. Metall.* **2**, 276–295 (2016).
41. Lin, X. *et al.* A novel application of hematite precipitation for high effective separation of Fe from Nd-Fe-B scrap. *Sci. Rep.* **9**, 1–8

(2019).

42. Jönsson, C. *et al.* The extraction of NdFeB magnets from automotive scrap rotors using hydrogen. *J. Clean. Prod.* **277**, 124058 (2020).

43. Rasheed, M. Z. *et al.* Review of the Liquid Metal Extraction Process for the Recovery of Nd and Dy from Permanent Magnets. *Metall. Mater. Trans. B* **52**, 1213–1227 (2021).

44. Li, X. Z. *et al.* A supramolecular lanthanide separation approach based on multivalent cooperative enhancement of metal ion selectivity. *Nat. Commun.* **9**, 547 (2018).

45. Jordens, A., Cheng, Y. P. & Waters, K. E. A review of the beneficiation of rare earth element bearing minerals. *Miner. Eng.* **41**, 97–114 (2013).

46. Chi, R., Li, Z., Peng, C., Gao, H. & Xu, Z. Preparation of enriched cerium oxide from bastnasite with hydrochloric acid by two-step leaching. *Metall. Mater. Trans. B Process Metall. Mater. Process. Sci.* **37**, 155–160 (2006).

47. Merritt, R. R. High Temperature Methods for Processing Monazite: II. Reaction with Sodium Carbonate. *J. Less-Common Met.* **166**, 211–219 (1990).

48. Woods, D. R. Appendix D: Capital Cost Guidelines. in *Rules of Thumb in Engineering Practice* 376–436 (Wiley-VCH Verlag GmbH & Co. KGaA, 2007). doi:10.1002/9783527611119.app4

49. Nuss, P. & Eckelman, M. J. Life cycle assessment of metals: a scientific synthesis. *PLoS One* **9**, e101298 (2014).

50. Skinner, B. J. Earth resources (minerals/metals/ores/geochemistry/mining). *Proc. Natl. Acad. Sci. USA* **76**, 4212–4217 (1979).

51. Jacob, K. T. & Iyengar, G. N. K. Thermodynamic study of Fe2O3-Fe2(SO4)3 equilibrium using an oxyanionic electrolyte (Na2SO4-I). *Metall. Trans. B* **17**, 323–329 (1986).

52. Hsieh, K. C. & Chang, Y. A. A solid-state emf study of ternary Ni-S-O, Fe-S-O, and quaternary Fe-Ni-S-O. *Metall. Trans. B* **17**, 133–146 (1986).

53. Dwivedi, R. K. & Kay, D. A. R. Thermodynamics of the oxidation of rare earth oxysulfides at high temperatures. *Metall. Trans. B* **15**, 523–528 (1984).

54. Akila, R., Jacob, K. T. & Shukla, A. K. Gibbs Energies of Formation of Rare Earth Oxysulfides. *Metall. Trans. B* **18B**, 163–168 (1987).

55. Dwivedi, R. K. Determination of the Thermodynamic Properties of Rare Earth-Oxygen-Sulfur Systems at High Temperatures. *PhD Thesis* (McMaster University, 1982).

56. Suponitskii, Y. L., Kuz'micheva, G. M. & Eliseev, A. A. Lanthanide Oxide Sulphides. *Russ. Chem. Rev.* **57**, 209–220 (1988).

57. Wang, M. Enthalpy of formation of LiNiO2, LiCoO2 and their solid solution, LiNi1−xCoxO2. *Solid State Ionics* **166**, 167–173 (2004).

58. Chang, K., Hallstedt, B. & Music, D. Thermodynamic and Electrochemical Properties of the Li−Co−O and Li−Ni−O Systems. *Chem. Mater.* **24**, 97–105 (2011).

59. Konings, R. J. M. *et al.* The Thermodynamic Properties of the f-Elements and their Compounds . Part 2 . The Lanthanide and Actinide Oxides The Thermodynamic Properties of the f -Elements and their Compounds . Part 2 . The Lanthanide and Actinide Oxides. *J. Phys. Chem. Ref. Data* **43**, 013101 (2014).

60. Kriklya, A. I., Bolgar, A. S. & Pribyl'skii, N. Y. Heat Capacity and Enthalpy of y-Dy2S3 Over a Wide Range of Temperature. *Sov. Powder Metall. Met. Ceram.* **31**, 697–700 (1992).

61. Chakraborti, N. Modified predominance area diagrams for the Fe-S-O system. *Can. J. Chem. Eng.* **61**, 763–765 (1983).

62. Madon, N. & Strickland-constable, R. F. Production of Carbon Disulfide. *Ind. Eng. Chem.* **50**, 1189–1192 (1958).

63. Fogler, H. S. *Elements of Chemical Reaction Engineering*. (Prentice Hall, 2016).

64. Sohn, H. Y. Review of fluid-solid reaction analysis—Part 2: Single porous reactant solid. *Can. J. Chem. Eng.* **97**, 2068–2076 (2019).

65. Sohn, H. Y. & Szekely, J. A structural model for gas-solid reactions with a moving boundary—III. *Chem. Eng. Sci.* **27**, 763–778 (1972).

66. Sohn, H. Y. & Szekely, J. The effect of intragrain diffusion on the reaction between a porous solid and a gas. *Chem. Eng. Sci.* **29**, 630–634 (1974).

67. Ishida, M. & Wen, C. Y. Comparison of kinetic and diffusional models for solid-gas reactions. *AIChE J.* **14**, 311–317 (1968).

68. Sohn, H. Y. & Perez-Fontes, S. E. Application of the Law of Additive Reaction Times to Fluid-Solid Reactions in Porous Pellets with Changing Effective Diffusivity. *Met. Mater. Trans. B* **41B**, 1261–1267 (2010).

69. Hirschfelder, J. O., Curtiss, C. F. & Bird, R. B. *Molecular Theory of Gases and Liquids*. (John Wiley & Sons Inc., 1954).

70. Berard, M. F., Wirkus, C. D. & Wilder, D. R. Diffusion of Oxygen in Selected Monocrystalline Rare Earth Oxides. *J. Am. Ceram. Soc.* **51**, 643–647 (1968).

71. Cussler, E. L. *Diffusion: Mass Transfer in Fluid Systems*. (Cambridge University Press, 2009).

72. Deen, W. M. *Introduction to Chemical Engineering Fluid Dynamics*. (Cambridge University Press, 2016).

73. Brown, A. M. & Ashby, M. F. Correlations for Diffusion Constants. *Acta Metall.* **28**, 1085–1101 (1980).

74. Liao, B. Q., Wan, C. R. & Wang, J. A Concept for the Estimation of HETS for Rare Earth Separations in Extraction Columns. *Sep. Sci. Technol.* **39**, 2597–2607 (2004).

75. Flett, D. S. Solvent extraction in hydrometallurgy: the role of organophosphorus extractants. *J. Organomet. Chem.* **690**, 2426–2438 (2005).

76. Towler, G. & Sinnott, R. *Chemical Engineering Design*. (Elsevier, 2013).

77. Cheng, C. Y. & Zhu, Z. Solvent extraction technology for the separation and purification of niobium and tantalum: A review. *Hydrometallurgy* **107**, 1–12 (2011).

78. Dincer, I. & Bicer, Y. *Mitacs Accelerate Project Final Report*. (2015).

79. Green, D. W. & Perry, R. H. *Perry's Chemical Engineer's Handbook*. (McGraw-Hill, 2008).

80. Christensen, P. & Dysert, L. *Cost Estimate Classification System as Applied in Engineering, Procurement, and Construction for the Process Industries*. *AACE International Recommended Practice No. 18R-97 COST, TCM Framework: 7.3 - Cost Estimating and Budgeting* (2005).

81. USGS. *Mineral Commodity Summaries 2021*. (2021).

82. USEIA & USDOE. *Annual Coal Report 2020*. (2021).

83. USEIA. *Henry Hub Natural Gas Spot Price*. (2021).

84. Misaka, T. & Mochizuki, Y. Recent Application and Running Cost of Moving Electrode type Electrostatic Precipitator. *Electrost. Precip.* 518–522 (2009). doi:10.1007/978-3-540-89251-9_103

85. Bleiwas, D. I. *Estimated Water Requirements for the Conventional Flotation of Copper Ores*. *USGS Open-File Report 2012-1089* (2012).

86. Bleiwas, D. I. *Estimates of Electricity Requirements for the Recovery of Mineral Commodities , with Examples Applied to Sub-Saharan Africa*. *USGS Open-File Report 2011-1253* (2011).

87. Bezuidenhout, G. A., Davis, J., van Beek, B. & Eksteen, J. J. Operation of a concentrated mode dual-alkali scrubber plant at the Lonmin smelter. *J. South. African Inst. Min. Metall.* **112**, 657–665 (2012).

88. King, M. J., Davenport, W. G. & Moats, M. S. *Sulfuric Acid Manufacture - Analysis, Control and Optimization*. (2013).

89. ISO. *ISO 14044*. (2006).

90. Ecoinvent-Association. ecoinvent 3.6. *Ecoinvent Center* (2019). Available at: www.ecoinvent.org.

91. Klett, C., Reeb, B., Missalla, M. & Schmidt, H.-W. Methods to Reduce Operating Costs in Circulating Fluidized Bed Calcination. in *Light Metals 2011* 125–130 (John Wiley & Sons, Inc., 2011). doi:10.1002/9781118061992.ch22

92. Fu, C. & Gundersen, T. Using exergy analysis to reduce power consumption in air separation units for oxy-combustion processes. *Energy* **44**, 60–68 (2012).

93. de Bakker, J. Energy Use of Fine Grinding in Mineral Processing. *Metall. Mater. Trans. E* **1**, 8–19 (2014).

94. USEPA. TRACI 2.1. *Tool for Reduction and Assessment of Chemicals and Other Environmental Impacts* (2014). Available at: https://www.epa.gov/chemical-research/tool-reduction-and-assessment-chemicals-and-other-environmental-impacts-traci.

95. USEIA. *Carbon Dioxide Emissions Coefficients*. (2021).

96. Stinn, C., Allanore, A. *Selective Sulfidation of Metal Compounds - Supporting Computing Files*. Harvard Dataverse Repository, Allanore Resaerch Group. (2021). https://doi.org/10.7910/DVN/193PW2